

Impact of magnetic field-driven anisotropies on the equation of state probed in neutron star mergers

ELIAS R. MOST,^{1,2} JEFFREY PETERSON,³ LUIGI SCURTO,⁴ HELENA PAIS,⁴ AND VERONICA DEXHEIMER³

¹TAPIR, Mailcode 350-17, California Institute of Technology, Pasadena, CA 91125, USA

²Walter Burke Institute for Theoretical Physics, California Institute of Technology, Pasadena, CA 91125, USA

³Department of Physics, Kent State University, Kent, OH 44243, USA

⁴CFisUC, Department of Physics, University of Coimbra, 3004-516 Coimbra, Portugal

ABSTRACT

Binary neutron star mergers can produce extreme magnetic fields, some of which can lead to strong magnetar-like remnants. While strong magnetic fields have been shown to affect the dynamics of outflows and angular momentum transport in the remnant, they can also crucially alter the properties of nuclear matter probed in the merger. In this work, we provide a first assessment of the latter, determining the strength of the pressure anisotropy caused by Landau level quantization and the anomalous magnetic moment. To this end, we perform the first numerical relativity simulation with a magnetic polarization tensor and a magnetic-field-dependent equation of state using a new algorithm we present here, which also incorporates a mean-field dynamo model to control the magnetic field strength present in the merger remnant. Our results show that – in the most optimistic case – corrections to the anisotropy can be in excess of 10%, and are potentially largest in the outer layers of the remnant. This work paves the way for a systematic investigation of these effects.

Keywords: Neutron stars (1108), General relativity(641), Nuclear astrophysics (1129), Nuclear physics (2077)

1. INTRODUCTION

From formation (A. P. Boss & S. A. Keiser 2013), through early life (A. Maeder & G. Meynet 2003; A. Igoshev et al. 2025) and supernova explosions (J. C. Wheeler et al. 2002; R. Raynaud et al. 2020; P. Barrère et al. 2022), to different stages of neutron star lives (M. Bejger et al. 2017; A. Y. Potekhin & G. Chabrier 2018; A. Bransgrove et al. 2018; S. K. Lander et al. 2021; A. G. Suvorov & J. A. Pons 2025; J.-L. Jiang et al. 2025), magnetic fields affect many aspects of stellar evolution. Magnetic fields of the order of 10^{16} G[¶] have been shown to noticeably deform fully evolved (beyond the proto-neutron star stage) neutron stars (R. O. Gomes et al. 2019). Nevertheless, magnetic fields need to be of the order of 10^{18} G to modify the thermodynamical relations (or equation of state, EoS) in the core of neutron stars and proto-neutron stars (D. Chatterjee et al. (2015); B.

Franzon et al. (2016); M. Strickland et al. (2012). In the crust, this threshold value is lower, $B \gtrsim 10^{15}$ G, which has been shown to affect the sub-saturation EoS, originating an extension of the inner crust (J. Fang et al. 2016, 2017a,b; S. Avancini et al. 2018; H. Pais et al. 2021; X. Wang et al. 2022; L. Scurto et al. 2023). Furthermore, strong modifications of the neutron star crust could have implications for wave launching (A. Bransgrove et al. 2020), crustal oscillations (J. A. Pons & D. Viganò 2019), and connections to radio transients (C. D. Bochenek et al. 2020; B. C. Andersen et al. 2020). So far, magnetic fields of up to $10^{15} - 10^{16}$ G have been identified in isolated neutron stars (magnetars) (V. M. Kaspi & A. Beloborodov 2017; K. Makishima et al. 2014, 2019, 2021, 2024) and even larger ones could be achieved in their cores (E. J. Ferrer et al. 2010).

Complementary to observing neutron stars, neutron star mergers (B. P. Abbott et al. 2017, 2020) have the potential to constrain properties for cold (K. Chatziioannou et al. 2018; C. Raithel et al. 2018; E. Annala et al. 2018; E. R. Most et al. 2018; B. P. Abbott et al. 2018; A. Bauswein et al. 2017; B. Margalit & B. D. Metzger 2017; L. Rezzolla et al. 2018; M. Ruiz et al. 2018; M. Shibata et al. 2019; A. Nathanail et al. 2021; H. Tan

[¶] To convert from Gauss (G) to Gaussian natural units, where the $\sqrt{4\pi}$ appears in the energy-momentum tensor, one can use $1 \text{ MeV}^2 = 1.44 \times 10^{13} \text{ G}$. To convert to Lorentz-Heaviside natural units, where the $\sqrt{4\pi}$ does not appear in the energy-momentum tensor, one can use $1 \text{ MeV}^2 = 5.11 \times 10^{13} \text{ G}$. Alternatively, $m_\pi^2/e \sim 3 \times 10^{18} \text{ G}$.

et al. 2020; E. R. Most et al. 2020; F. J. Fattoyev et al. 2020) and hot nuclear matter (A. Bauswein et al. 2010; A. Perego et al. 2019; A. Figura et al. 2020; C. Raithel et al. 2021; J. Fields et al. 2023; C. A. Raithel & V. Paschalidis 2024, 2023; V. Villa-Ortega et al. 2023; M. Miravet-Tenés et al. 2024), including the effect of neutrinos (M. G. Alford et al. 2018; E. R. Most et al. 2021; F. Zappa et al. 2022; P. L. Espino et al. 2024; E. R. Most et al. 2024). One aspect that has so far been neglected in neutron-star merger simulations is the feedback of strong magnetic fields on the EoS, which has been addressed in isolated stars in many works (E. S. Fraga & A. J. Mizher 2008; M. Orsaria et al. 2011; E. V. Gorbar et al. 2011; V. Dexheimer et al. 2012; R. Aguirre et al. 2014; M. Sinha et al. 2013; P.-C. Chu et al. 2015; A. Haber et al. 2016; R. Aguirre & E. Bauer 2015; A. A. Isayev 2014; N. Chamel et al. 2015; D. A. Fogaça et al. 2016; L. Tolos et al. 2017; V. Dexheimer et al. 2017; S. Avancini et al. 2018; G. Lugones & A. G. Grunfeld 2019; A. Mishra et al. 2019; D. Chatterjee et al. 2019; P. M. Lo et al. 2020; E. J. Ferrer & A. Hackebill 2022; B. C. T. Backes et al. 2021; Z.-Y. Lu et al. 2022; R. Prasad & R. Mallick 2022; O. G. Benvenuto et al. 2023; J. Peterson et al. 2023; R. Mondal et al. 2024a; Y. Wang & X.-J. Wen 2024; R. Mondal et al. 2024b; M. Kawaguchi et al. 2025). While such effects commonly appear only at magnetic fields above 10^{15} G, making them subdominant for most isolated neutron stars, the merger of two neutron stars has been shown to feature dynamo amplification capable of magnetic fields in excess of this limit within milliseconds after merger (D. Price & S. Rosswog 2006; K. Kiuchi et al. 2015).

Using numerical relativity simulations, these dynamo processes have been investigated extensively using either ab-initio (K. Kiuchi et al. 2018; R. Aguilera-Miret et al. 2022; M. Chabanov et al. 2023; R. Aguilera-Miret et al. 2023; K. Kiuchi et al. 2024) or sub-grid dynamo approaches (B. Giacomazzo et al. 2015; C. Palenzuela et al. 2015; E. R. Most & E. Quataert 2023; E. R. Most 2023) to produce strong field strengths. While the background dynamics of magnetic fields in mergers (including winding and breaking (S. L. Shapiro 2000)) have been extensively investigated (M. Anderson et al. 2008; B. Giacomazzo et al. 2011; B. Giacomazzo & R. Perna 2013; K. Kiuchi et al. 2014; C. Palenzuela et al. 2015; A. Endrizzi et al. 2016; T. Kawamura et al. 2016; R. Ciolfi et al. 2017; L. Combi & D. M. Siegel 2023a; J. Bamber et al. 2025; E. M. Gutiérrez et al. 2025), only recently has it been realized that strong magnetic field in the outer layers of the neutron star can aid the launching of magnetically driven winds, jets and flares (E. R. Most & E. Quataert 2023; L. Combi & D. M. Siegel 2023b; K.

Kiuchi et al. 2024; E. R. Most 2023; J.-L. Jiang et al. 2025; C. Musolino et al. 2024; J. Bamber et al. 2024), potentially affecting the electromagnetic afterglow (B. D. Metzger et al. 2018; P. Mösta et al. 2020; S. Curtis et al. 2024; L. Combi & D. M. Siegel 2023b). Magnetic fields might also impact angular momentum transport inside the remnant (B. Margalit et al. 2022; A. Tsokaros et al. 2025; J. Bamber et al. 2025; A. Reboul-Salze et al. 2024). This necessarily requires the outer layers of the magnetar merger remnant to reach field strengths in excess of 10^{16} G (K. Kiuchi et al. 2024; E. R. Most 2023).

In this work we provide a first investigation of the impact magnetic fields could have on the EoS in neutron star mergers. To decrease the model dependency of our work, we study different EoS combinations to model entire neutron stars, from outer crusts to inner cores, including magnetic-field effects, both from Landau quantization and anomalous magnetic moment (AMM) corrections. Using these equations of state, we then perform fully general-relativistic neutron star mergers simulations with a magnetic polarization tensor and a mean-field dynamo prescription to control the amount of magnetic field amplification produced in the merger. This allows us to systematically vary the field strength in different regions of the merger to disentangle the inherent modifications to the dynamics due to the mere inclusion of strong magnetic fields from the specific feedback on the EoS they may have.

2. EQUATION OF STATE DESCRIPTION

To construct different EoSs, we combine different crust descriptions for the lower density part (containing nuclei, referred to as the crust) and different descriptions for the higher density part (with bulk matter, referred to as the core), to obtain two complete description of neutron stars including the effects of strong magnetic fields: Landau quantization and anomalous magnetic moment (AMM). Note that not many EoSs are available that include magnetic field effects, especially including the AMM. The details on the EoSs we use are given in Appendix A, but we summarize them here, and discuss how they generate magnetic-field induced anisotropies in dense matter in the following.

In this study we use two different models: NL3 $\omega\rho$ (C. J. Horowitz & J. Piekarewicz 2001a,b; H. Pais & C. Providência 2016) and CMF (V. Dexheimer & S. Schramm 2008; V. Dexheimer et al. 2012).

The NL3 $\omega\rho$ is a Walecka-type of relativistic model (H. Mueller & B. D. Serot 1996; B. D. Serot & J. D. Walecka 1986) that describes nucleons (protons and neutrons) interacting through a mean-field of three mesons: the scalar isoscalar σ , the vector isoscalar ω and the vector

isovector ρ . This model is based on the NL3 interaction (G. A. Lalazissis et al. 1997), where the additional $\omega\rho$ term was added to ensure a better agreement with astrophysical data (V. Dexheimer et al. 2019), by modeling the density dependence of the symmetry energy (H. Pais & C. Providência 2016). For the crust, we combine an inner crust calculated from a compressible liquid drop model (see e.g. J. M. Lattimer et al. (1985); J. M. Lattimer & F. D. Swesty (1991); G. Baym et al. (1971); S. S. Bao et al. (2014); H. Pais et al. (2015)) under strong magnetic fields (L. Scurto et al. 2023) with a smooth transition to a SLy4 outer crust (F. Douchin & P. Haensel 2001).

We also use a hadronic version of the Chiral Mean Field (CMF) model. It is a relativistic model that describes the baryon octet (nucleons and hyperons) also interacting through a mean field of mesons, but now reproducing chiral symmetry restoration (V. Dexheimer & S. Schramm 2008; V. Dexheimer et al. 2012). We combine it with the SLy4 EoS for the outer crust (F. Douchin & P. Haensel 2001).

To highlight how the magnetic field affects differently each core EoS, we show in Fig. 1 two-dimensional contours for the pressure anisotropy due to the magnetic field as a function of magnetic-field strength B and baryon (number) density n_B . We do not extend the figure to very low densities because the outer crust we use does not support a pressure anisotropy. The pressure anisotropy is defined as the difference between the pressure in the local direction of the magnetic field (parallel pressure) and in the direction perpendicular to it (perpendicular pressure), normalized by the parallel pressure, i.e., $(P_{\parallel} - P_{\perp})/P_{\parallel}$, where the parallel pressure corresponds to the thermodynamic pressure. In the low magnetic field limit, the anisotropy goes to 0 (equal pressures, shown in black), while in the extremely high magnetic field case, it goes to 1 and above (zero perpendicular pressure, shown in orange and negative pressure anisotropy, shown in yellow). The figure shows that the stronger the field, the higher the density it can modify the EoS, with stronger effects overall for the CMF model, which contains hyperons. The color oscillations are caused by the Van Alphen oscillations due to the discrete nature of the Landau levels (W. J. De Haas & P. M. Van Alphen 1930).

3. GENERAL-RELATIVISTIC MAGNETOHYDRODYNAMICS WITH MAGNETIC POLARIZATION

In this study, we solve the equations of general-relativistic magnetohydrodynamics for use with the magnetic field dependent EoSs described in Sec. 2. Most

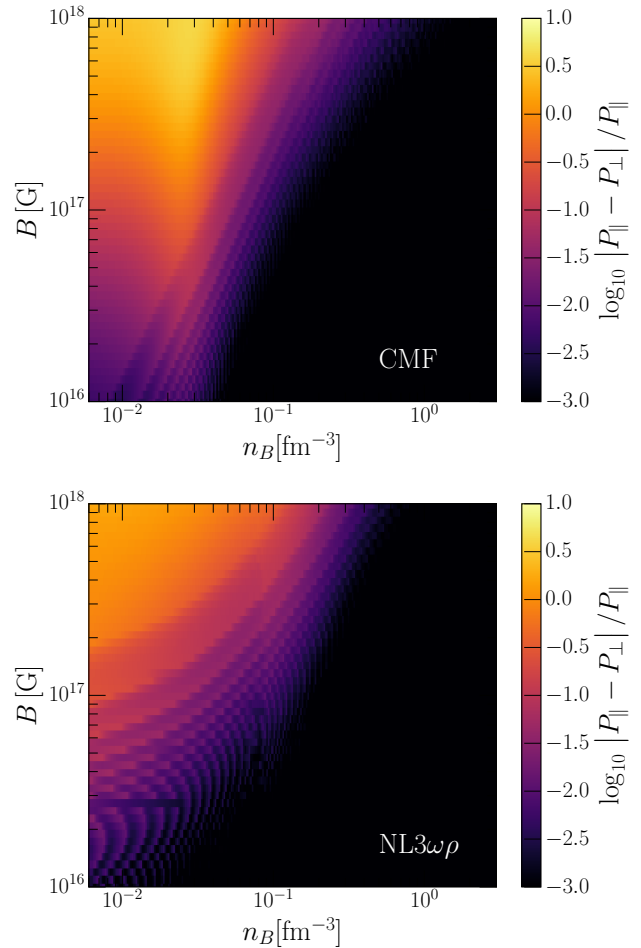


Figure 1. Normalized pressure anisotropy, $(P_{\parallel} - P_{\perp})/P_{\parallel}$, due to the magnetic field as a function of magnetic-field strength, B , and baryon number density, n_B , for the CMF model (top panel) and the NL3 $\omega\rho$ model (bottom panel). The parallel pressure component, P_{\parallel} , is the thermodynamic pressure, P_{\perp} is the perpendicular pressure.

importantly, we also provide a simple way for including magnetic polarization into the equations we solve (D. Chatterjee et al. 2015; O. M. Pimentel et al. 2018). In the following, we largely adopt the language of the 3+1 formulation of general-relativity (e.g., E.ourgoulhon (2007)). Consequently, we decompose the spacetime metric as,

$$ds^2 = g_{\mu\nu} dx^\mu dx^\nu = (-\alpha^2 + \beta_i \beta^i) + 2\beta_i dt dx^i + \gamma_{ij} dx^i dx^j, \quad (1)$$

where α is the lapse, β^i the shift vector, and γ_{ij} the induced three-metric on the hypersurface defined by the normal vector, $n_\mu = (-\alpha, 0, 0, 0)$. We model the dynamics of matter using general-relativistic magnetohydrodynamics in dynamical spacetimes (T. W. Baumgarte & S. L. Shapiro 2003; M. D. Duez et al. 2005). Mat-

ter is described in terms of an energy density e , pressure P and four-velocity u^μ . Within the 3+1 split, we can define a three-vector velocity $v_i = Wu_i$, such that $W = 1/\sqrt{1 - v_i v^i}$ is the Lorentz factor.

The electromagnetic sector is described by the vector potential,

$$\mathcal{A}_\mu = \Phi n_\mu + A_\mu, \quad (2)$$

where A_i is the spatial component, and Φ the gauge potential. This gives rise to the the field strength tensor,

$$F_{\mu\nu} = \nabla_\mu A_\nu - \nabla_\nu A_\mu, \quad (3)$$

where ∇_μ is the four-dimensional covariant derivative, and its dual $*F^{\mu\nu} = -\frac{1}{2}\varepsilon^{\mu\nu\kappa\lambda}F_{\kappa\lambda}$. We can then define electric and magnetic fields in the normal and co-moving frame, via, $E^\mu = n_\nu F^{\mu\nu}$, $B^\mu = n_\nu *F^{\mu\nu}$, and $e^\mu = u_\nu F^{\mu\nu}$, $b^\mu = u_\nu *F^{\mu\nu}$, respectively.

We then assume the ideal magnetohydrodynamics approximation, $e^\mu \approx 0$, appropriate for the highly electrically conductive regime probed in neutron star mergers (A. Harutyunyan et al. 2018). However, since we want to control dynamo amplification in the merger remnant, we supplement it with a mean-field dynamo term (E. R. Most 2023),

$$e^\mu = \kappa b^\mu, \quad (4)$$

where κ is the dynamo coefficient (N. Bucciantini & L. Del Zanna 2013). This translates to a normal electric field (E. R. Most 2023),

$$E^i = -\varepsilon^{ijk}v_j B_k + \kappa [(1 - v^2) B^i + (v_l B^l) v^i] + \mathcal{O}(\kappa^2). \quad (5)$$

Overall, this leads to a final evolution equation (E. R. Most 2023),

$$\begin{aligned} \partial_t A_i &= \frac{\alpha}{u^0} \varepsilon_{ijk} u^j B^k - \alpha \kappa [(1 - v^2) B_i + (v_l B^l) v_i] \\ &\quad - \partial_i (\alpha \Phi - \beta^j A_j), \end{aligned} \quad (6)$$

where the magnetic field follows from $B^i = \varepsilon^{ijk} \partial_j A_k$, and ε^{ijk} is the Levi-Civita tensor on the hypersurface.

The energy momentum tensor of the resulting dynamo system is identical to ideal magnetohydrodynamics up to the order we consider (E. R. Most 2023),

$$\begin{aligned} T_{\text{ideal}}^{\mu\nu} &= (\varepsilon + P + b^2) u^\mu u^\nu + \left(P + \frac{1}{2}b^2\right) g^{\mu\nu} - b^\mu b^\nu \\ &\quad + \mathcal{O}(\kappa^2), \end{aligned} \quad (7)$$

where ε and P (or P_\parallel) in our simulations comes from Eqs. (A52) and (A53) for CMF and Eqs. (A27), (A20) and (A24) for NL3 $\omega\rho$.

Additionally, it has been shown that the presence of strong magnetic fields introduces an anisotropy in the pressure. This can be captured by tracking the magnetic polarization of the material in terms of a polarization vector m^μ (D. Chatterjee et al. 2015). The full energy momentum tensor of a polarizable magnetohydrodynamical fluid is given as

$$T^{\mu\nu} = T_{\text{ideal}}^{\mu\nu} + T_{\text{mag}}^{\mu\nu}, \quad (8)$$

where we now have a correction (D. Chatterjee et al. 2015; O. M. Pimentel et al. 2018),

$$T_{\text{mag}}^{\mu\nu} = \frac{1}{2} [m^\mu b^\nu + m^\nu b^\mu] - [u^\mu u^\nu + g^{\mu\nu}] b^\alpha m_\alpha. \quad (9)$$

giving rise to a perpendicular pressure (P_\perp), which for our scenario comes from Eq. (A54) for CMF and Eq. (A25) for NL3 $\omega\rho$. We now assume that the polarization aligns with co-moving magnetic field, i.e.,

$$m^\mu = \mu b^\mu, \quad (10)$$

where $\mu = (P_\perp - P_\parallel) / b^2$ is the magnetic susceptibility.

The non-ideal correction then takes a Braginskii-like form (M. Chandra et al. 2015; E. R. Most & J. Noronha 2021)

$$T_{\text{mag}}^{\mu\nu} = -\frac{2}{3}\mu b^2 \Delta^{\mu\nu} + \mu \left(b^\mu b^\nu - \frac{1}{3} \Delta^{\mu\nu} b^2 \right), \quad (11)$$

corresponding to a bulk pressure and anisotropic pressure correction. However, different from Braginskii theory the anisotropy is not evolved, but provided by the EoS. This allows us to apply a fluid-frame transformation to recast the equation as closely as possible to ideal MHD. This results in the effective system,

$$T^{\mu\nu} = \left(\tilde{e} + \tilde{P} + \tilde{b}^2 \right) u^\mu u^\nu + \left(\tilde{P} + \frac{1}{2} \tilde{b}^2 \right) g^{\mu\nu} - \tilde{b}^\mu \tilde{b}^\nu, \quad (12)$$

where

$$\tilde{b}^\mu = \sqrt{1 - \mu} b^\mu, \quad (13)$$

$$\tilde{e} = e - \frac{\mu}{2(1 - \mu)} \tilde{b}^2 = e - \frac{P_\perp - P_\parallel}{2}, \quad (14)$$

$$\tilde{P} = P_\parallel - \frac{\mu}{2(1 - \mu)} \tilde{b}^2 = \frac{3}{2} P_\parallel - \frac{1}{2} P_\perp. \quad (15)$$

The evolution of the system we solve is then governed by

$$\nabla_\mu (\rho u^\mu) = 0, \quad (16)$$

$$\nabla_\mu T^{\mu\nu} = 0, \quad (17)$$

$$\nabla_\mu *F^{\mu\nu} = 0, \quad (18)$$

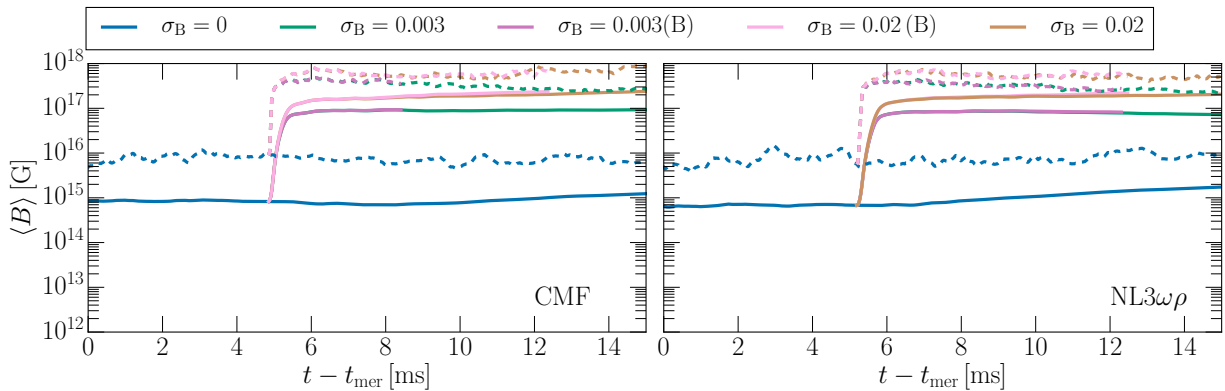


Figure 2. Evolution of the magnetic field strength, B , during and after merger. Shown are mass-weighted averages (solid lines) and maximum values (dashed lines) for both equations of state, CMF and $\text{NL}3\omega\rho$, where ‘B’ indicates feedback of the magnetic field onto the equation of state. σ_B indicates the magnetization for saturation of the mean-field dynamo. Times, t , are stated relative to the time of merger, t_{mer} .

where $\rho = m_B n_B$ is the baryon rest-mass density, m_B is the baryon mass.

We can gain some insights into the meaning of this pressure correction by using the language of out-of-equilibrium hydrodynamics P. Romatschke (2010). We can see that this transformation is akin to choosing a generalized hydrodynamic frame, which features out-of-equilibrium energy and pressure corrections, $\tilde{P} = P_{\parallel} + \Pi$ (J. Noronha et al. 2022; G. S. Rocha & G. S. Denicol 2021). In particular, we may use that the pressure anisotropy, Π , takes the form of an effective bulk pressure correction,

$$\Pi = \frac{1}{2} (P_{\parallel} - P_{\perp}) , \quad (19)$$

which satisfies

$$u^{\mu} \nabla_{\mu} \Pi = - \left(\rho \frac{\partial \Pi}{\partial \rho} \Big|_{b^2} + 2b^2 \frac{\partial \Pi}{\partial b^2} \Big|_{\rho} \right) \nabla_{\mu} u^{\mu} + 2 \frac{\partial \Pi}{\partial b^2} \Big|_{\rho} b_{\mu} b_{\nu} \sigma^{\mu\nu} , \quad (20)$$

where $\sigma_{\mu\nu}$ is the shear tensor. Different from, e.g., neutrino-driven bulk viscosity (E. R. Most et al. 2021, 2024; L. Gavassino & J. Noronha 2024), the pressure anisotropy is a non-dissipative (damping) effect. As we will see, the anisotropy largely builds up due to increase in magnetic field strength after the initial collision and core bounces, where compression is largest (V. Nedora et al. 2021). As such, the anisotropy is purely sourced by shear-driven (dynamo) amplification of the magnetic field

$$u^{\mu} \nabla_{\mu} \Pi \approx 2 \frac{\partial \Pi}{\partial b^2} \Big|_{\rho} b_{\mu} b_{\nu} \sigma^{\mu\nu} , \quad (21)$$

where the above holds approximately in the conditions of the post-merger.

While magneto-turbulence is prevalent throughout the entire remnant after merger (R. Aguilera-Miret et al. 2022), the saturation of the dynamo requiring near-equipartition values for the anisotropy to become dynamically important, $\Pi \gtrsim P_{\parallel}$. This makes the outer layers of the merger remnant, where a turbulent $\alpha\Omega$ -dynamo operates (K. Kiuchi et al. 2024), a most promising site, as the field strength there easily reach equipartition (E. R. Most 2023), aiding breakout of the field from the surface of the star (E. R. Most & E. Quataert 2023; L. Combi & D. M. Siegel 2023b; E. R. Most 2023; C. Musolino et al. 2024).

4. NUMERICAL IMPLEMENTATION

We numerically solve the equations of ideal GRMHD with polarizable matter in dynamical spacetimes using the Frankfurt/IllinoisGRMHD (FIL) code (E. R. Most et al. 2019), and its recently developed dynamo infrastructure (E. R. Most 2023). In detail, we solve the Einstein field equations in the Z4c formulation (S. Bernuzzi & D. Hilditch 2010; D. Hilditch et al. 2013) in moving puncture gauge (M. Alcubierre et al. 2003) using a fourth-order accurate finite-difference discretization (Y. Zlochower et al. 2005). The GRMHD equations are solved using a fourth-order accurate variant of the conservative finite-difference scheme ECHO scheme (L. Del Zanna et al. 2007), including a robust primitive inversion scheme for high magnetization (W. Kastaun et al. 2021), which we have modified for use with the magnetic field dependent EoSs, see Appendix B. The equations of state are tabulated. Additional details on the code and setup can be found in E. R. Most et al. 2019; E. R. Most & C. A. Raithel 2021; C. A. Raithel & E. R. Most 2022.

We consider different magnetic-field-dependent equations of state at zero-temperature, CMF and $\text{NL}3\omega\rho$, as

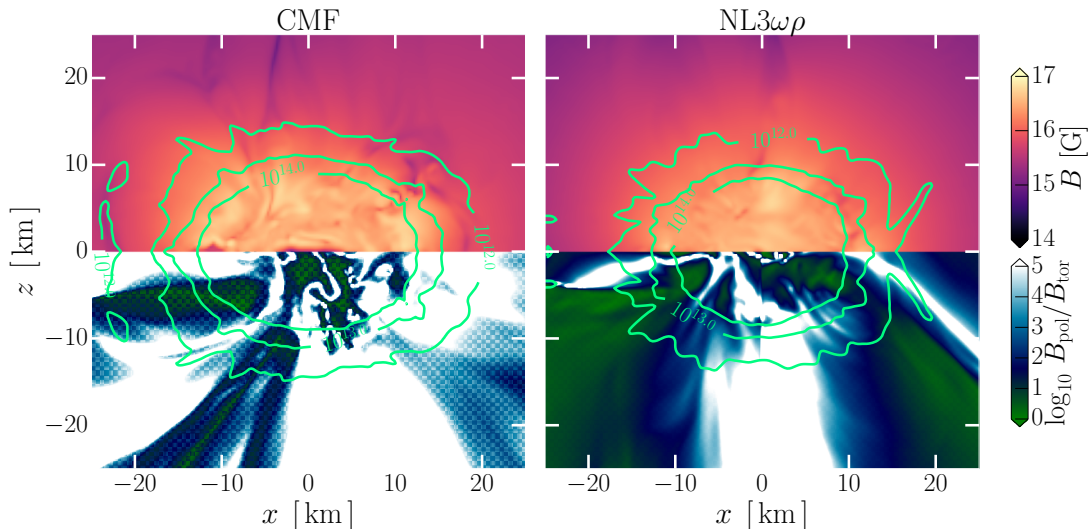


Figure 3. Hypermassive neutron star using the CMF and $NL3\omega\rho$ equations of state about 12 ms after merger. Shown is the absolute magnetic field strength, B , (top panels) and the ratio of poloidal, B_{poloidal} , and toroidal, B_{toroidal} , magnetic field (bottom panels). Green contour lines indicate level surfaces of the baryon rest-mass density ρ_B in g/cm^3 .

described in Sec. 2. In order to compare the effect of magnetic field dependence, we perform two sets of simulations, one with magnetic field feedback included, the other one fixed to its zero magnetic field slice. For these sets of simulations the impact of pressure anisotropy is then only estimated in post-processing. We also use two dynamo amplification parameters, such that the dynamo saturates at a given level of target magnetization $\sigma_B = b^2/\rho = \{0.003; 0.02\}$ (E. R. Most & E. Quataert 2023). The initial data for our simulations is computed using the FUKA/Kadath library (L. J. Papenfort et al. 2021; P. Grandclement 2010). Specifically we adopt non-spinning equal mass configurations with a total mass of $2.6 M_\odot$. We further adopt a simulation domain spanning $[-2, 048 : 2, 048]$ km over 8 refinement levels, with a finest resolution of 250 m.

5. RESULTS

In this work, we want provide a first assessment of the impact of magnetic-field driven pressure anisotropies in binary neutron star mergers. Before presenting this main result of our study (Sec. 5.1), we provide a brief description of the merger dynamics, which has largely been investigated in previous work (see, e.g., K. Kiuchi (2025) for a recent review).

During the merger of two neutron stars, a shear layer develops at the contact interface (D. Price & S. Rosswog 2006; L. Baiotti et al. 2008). It has been demonstrated that this shear layer, together with the onset of turbulence throughout the merger remnant leads to an amplification of initially weak magnetic fields to values of 10^{17} G in the central regions of the merger remnant (K. Kiuchi et al. 2015; C. Palenzuela et al. 2022; R.

Aguilera-Miret et al. 2023). After the merger, a remnant develops which has a nearly uniformly rotating inner core, a rapidly rotating outer layer with radially increasing angular velocity, and a Keplerian envelope at crustal densities (M. Hanauske et al. 2017). This latter part has been shown to be unstable to the magnetorotational instability, developing an effective $\alpha\Omega$ -dynamo (K. Kiuchi et al. 2024), that can drive the outer layers to an equipartition state between the magnetic field energy and the fluid, leading to an effective breakout of the field from the star (E. R. Most & E. Quataert 2023; L. Combi & D. M. Siegel 2023b). As a consequence, those regions are in a regime where magnetic field corrections to the EoS could become important, although we caution that finite-temperature effects (which we do not self-consistently capture) may alter this picture (M. Strickland et al. 2012).

Since our simulations are not able to fully capture the dynamo amplification self-consistently, we utilize a mean-field dynamo model (E. R. Most 2023) to mimic the amplification process outlined above. Starting from the post-merger remnant around $t = 5$ ms after merger (Fig. 2), we activate the mean-field dynamo term, and drive the system into a state of constant magnetization $\sigma_B = b^2/\rho = \{0.003; 0.02\}$ (see, e.g., (E. R. Most & E. Quataert 2023; E. R. Most 2023), which we vary to capture different magnetic field amplification strengths. Note that subsequent self-consistent evolution after the dynamo term is deactivate will further enhance the magnetic field strength, making it overall more similar for both configurations. We generally consider two cases: In the first case, we consider dynamical evolutions using

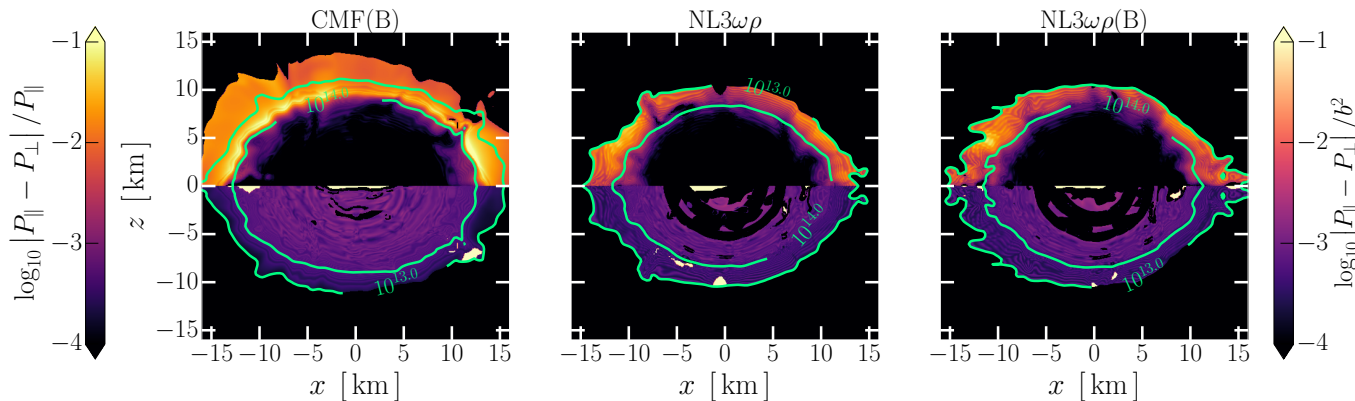


Figure 4. Normalized pressure anisotropy, $(P_{\parallel} - P_{\perp})/P_{\parallel}$, (top panels) and magnetic susceptibility, $\mu = (P_{\parallel} - P_{\perp})/b^2$, (bottom panels) shown at 8 ms after merger for the CMF and NL3 $\omega\rho$ equation of state. b^2 denotes the local magnetic field energy in the comoving frame. We show results for the equation of state (EOS) with magnetic field dependence ('B'), and post-processed when simulating only with the $B = 0$ EOS.

the $B = 0$ part of the EoS, and then estimate in post-processing how large the pressure anisotropy would be. In the second part, we perform fully backreacted simulations using the magnetic field dependent EoS and the polarization tensor. The subsequent evolution beyond this initial saturation proceeds self-consistently in ideal GRMHD. We show this evolution in Fig. 2, where we depict the mass weighted average $\langle B \rangle$ of the magnetic field strength. As soon as we activate the dynamo, the magnetic field inside the remnant is quickly amplified. Since we choose a uniform σ_B amplification (E. R. Most & E. Quataert 2023), rather than a sophisticated model for the $\alpha\Omega$ -dynamo (E. R. Most 2023), the field strength is amplified throughout the remnant and quickly saturates.

The overall evolution is relatively insensitive to the EoS, barring intrinsic differences due to changes in stellar structure. In general, we find that without the addition of a dynamo term, our simulations saturate at field strengths between $10^{15} - 10^{16}$ G. If a mean-field dynamo term is included, we easily reach average magnetic field strengths of $10^{16} - 10^{17}$ G inside the remnant. The maximum field strength probed, depends on the exact dynamo saturation value and is in excess of 10^{17} G, which is sufficient to trigger pressure anisotropies as discussed in Sec. 2. Since the pressure anisotropy depends critically on the magnetic field topology, Fig. 3 shows the relative ratio of poloidal, B_{poloidal} and toroidal, B_{toroidal} , field inside the magnetar remnant. We can see that the remnant features a mix of toroidal and poloidal field, with strong poloidal fields present at the surface of the neutron star, leading to breakout of the field from the remnant (E. R. Most & E. Quataert 2023; L. Combi & D. M. Siegel 2023b; C. Musolino et al. 2024).

5.1. Pressure anisotropy

Owing to the large magnetic field strength we drive in the hypermassive neutron star, a net Braginskii-like pressure anisotropy, $(P_{\parallel} - P_{\perp})$ builds up in the system, as can be seen from Eq. (21). We quantify this pressure anisotropy around 8 ms after merger in Fig. 4. We can see that for sufficient magnetic field amplification, pressure anisotropies of order unity can be probed in the outer layers of the remnant. While they are also present at high density, the magnetic field strengths we probe there are further away from their equipartition values (E. R. Most 2023), leading to only small anisotropies of order $\Pi \simeq 10^{-3} - 10^{-4} P_{\parallel}$, with the spread being determined by the choice of equation of state. We caution that, overall, this strongly depends on the magnetic field strengths produced in the merger, which can be larger than what we use here (K. Kiuchi et al. 2018; R. Aguilera-Miret et al. 2022).

In Fig. 5, we also quantify the temporal evolution of the pressure anisotropy. As demonstrated in Eq. (21), the anisotropy does not necessarily decay, except if the field was strongly sheared apart. This makes this effect unlike conceptually similar pressure corrections, such as Urca-driven bulk viscosity (E. R. Most et al. 2021, 2024). Accordingly, we find that the average pressure anisotropy initially increases during merger, reaching values of $\Pi \simeq 10^{-3} P_{\parallel}$ primarily inside the core. Such values are likely too small to affect the subsequent evolution of the system, as they are smaller than thermal (A. Figura et al. 2020; C. Raithel et al. 2021; J. Fields et al. 2023) and bulk viscous corrections (E. R. Most & C. A. Raithel 2021; E. R. Most et al. 2024). However, inside the crustal regions of the remnant, anisotropies can reach between $\Pi \simeq (10^{-2} - 10^{-1}) P_{\parallel}$ (as we have seen in Fig. 4). Overall, we can see that the evolution of the

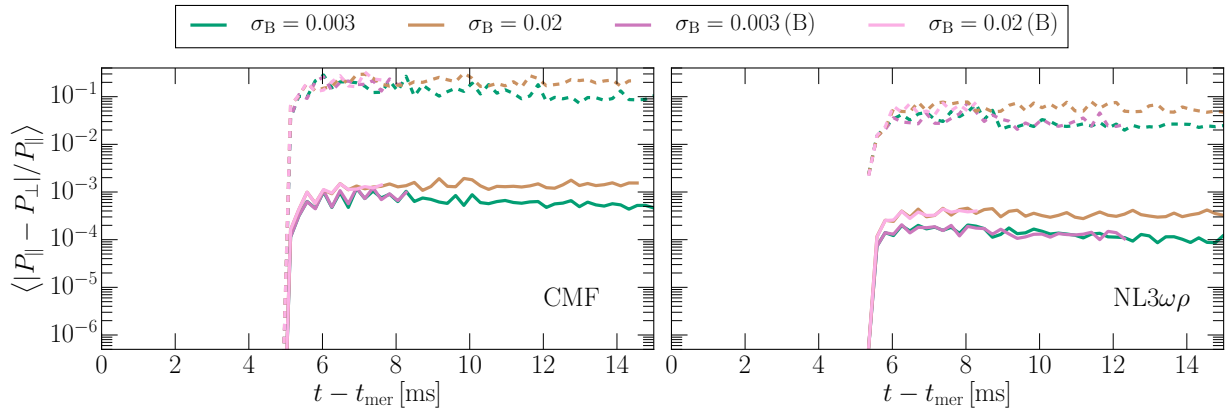


Figure 5. Magnetic pressure anisotropy inside the magnetar remnant. Shown are mass-weighted averages (solid lines) and maximum values (dashed lines) for both equations of state, CMF and NL3 $\omega\rho$. The maximum values are always located inside the crust region, whereas the mass-weighted averaged provide a faithful representation inside the core. Different colors denote dynamo saturation levels in terms of the magnetization σ_B . The letter ‘B’ indicates a simulation with magnetic field feedback on the equation of state included.

anisotropy, both maximum values (in the crust) and average values (in the core), are comparable between the two sets of simulations including the backreaction of the field on the EoS or not. These conclusions seem largely independent of the high-density EoS, and primarily depend on physics below saturation densities, which for the densities considered for this effect is different for the two systems considered. We caution, however, that we neglect finite-temperature corrections to the EoS, which naturally lowers the expected anisotropy. As such our results, should be seen as an upper bound of this effect.

6. CONCLUSIONS

Magnetic fields in neutron star mergers can be amplified to magnetar-level field strengths (K. Kiuchi et al. 2018; R. Aguilera-Miret et al. 2023; K. Kiuchi et al. 2024; E. R. Most 2023). For those values, the magnetic field can become large enough to affect the properties of dense matter via Landau level quantization, and the anomalous magnetic moment (W. J. De Haas & P. M. Van Alphen 1930). We have presented the first assessment of this anisotropy on the post-merger dynamics of a binary neutron star coalescence. In doing so, we have incorporated a polarization tensor into the GRMHD equations using the formulation of D. Chatterjee et al. (2015), which allows us to control the pressure anisotropy present in nuclear matter. We have then used two different descriptions of nuclear matter, CMF and NL3 $\omega\rho$, both of which include an effective magnetic field dependence and a crust. By performing fully general-relativistic simulations of binary neutron star coalescence, we demonstrated that after merger magnetic fields, in particular in the outer regions of the merger remnant become strong enough to reach the threshold for magnetic field anisotropies to po-

tentially become dynamically important. We find that locally the anisotropy can reach values of 10%, for the strongest magnetic field amplification strength in the post-merger remnant (this number is EoS dependent), which in the relevant regions is largely driven by the $\alpha\Omega$ -dynamo (K. Kiuchi et al. 2024; E. R. Most 2023). Since these regions are susceptible to eventual breakout of the magnetic field from the star by means of Parker instabilities (E. R. Most & E. Quataert 2023; L. Combi & D. M. Siegel 2023b; K. Kiuchi et al. 2024; C. Musolino et al. 2024; J.-L. Jiang et al. 2025), the anisotropy may change the dynamics of jet and wind launching from these systems. A detailed analysis of this aspects will be presented in future work. One aspect not presently addressed is the temperature dependence of the anisotropy (M. Strickland et al. 2012). Our initial assessment has so far relied on a fixed cold segment of the EoS, that was augmented with a thermal component, which did not couple to the magnetic field. A self-consistent analysis should be carried out in future work to clarify this dependence.

7. ACKNOWLEDGMENTS

The authors are grateful for discussions with Constança Providência and Ira Wasserman. ERM acknowledges support from NASA’s ATP program under grant 80NSSC24K1229 and by the National Science Foundation under grants No. PHY-2309210. The work of LS and HP was partially supported by national funds from FCT (Fundação para a Ciência e a Tecnologia, I.P, Portugal) under projects UIDB/04564/2020 and UIDP/04564/2020, with DOI identifiers 10.54499/UIDB/04564/2020 and 10.54499/UIDP/04564/2020, respectively, and the project 2022.06460.PTDC with the associ-

ated DOI identifier 10.54499/2022.06460.PTDC. LS acknowledges the PhD grant 2021.08779.BD (FCT, Portugal). HP acknowledges the grant 2022.03966.CEECIND (FCT, Portugal) with DOI identifier 10.54499/2022.03966.CEECIND/CP1714/CT0004. V.D. acknowledges support from the Department of Energy under grant DE-SC0024700 and from the National Science Foundation under grants MUSES OAC-2103680 and NP3M PHY2116686. ERM acknowledges the use of Delta at the National Center for Supercomputing Applications (NCSA) through allocation PHY210074 from the Advanced Cyberinfrastructure Coordination Ecosystem: Services & Support (ACCESS) program, which is supported by National Science Foundation grants #2138259, #2138286, #2138307, #2137603, and #2138296. Additional simulations were

performed on the NSF Frontera supercomputer under grant AST21006. ERM also acknowledges support through DOE NERSC supercomputer Perlmutter under grant m4575, which uses resources of the National Energy Research Scientific Computing Center, a DOE Office of Science User Facility supported by the Office of Science of the U.S. Department of Energy under Contract No. DE-AC02-05CH11231 using NERSC award NP-ERCAP0028480.

Software: EinsteinToolkit (F. Loffler et al. 2012), Frankfurt/IllinoisGRMHD (E. R. Most et al. 2019; Z. B. Etienne et al. 2015) FUKA (L. J. Papenfort et al. 2021), Kadath (P. Grandclement 2010), kuibit (G. Bozzola 2021), matplotlib (J. D. Hunter 2007), numpy (C. R. Harris et al. 2020), scipy (P. Virtanen et al. 2020)

APPENDIX

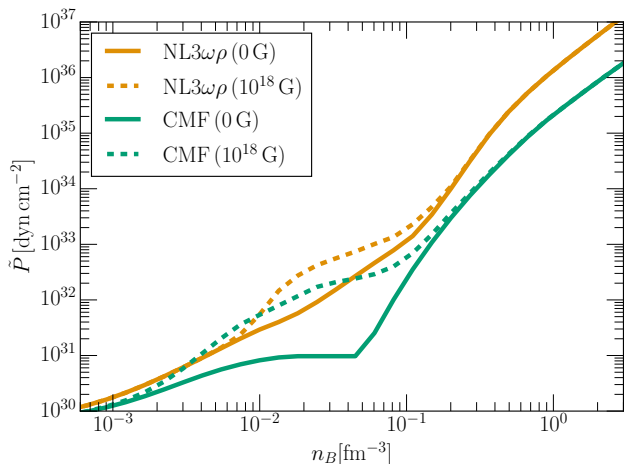


Figure A.1. Equations of state used in this work. Shown are the *CMF*, *NL3 $\omega\rho$* models, with dashed lines indicating strong magnetic field impacts. The pressure shown is the effective pressure, $\tilde{P} = (3/2)P_{\parallel} - (1/2)P_{\perp}$, as a function of baryon number density n_B .

A. EQUATIONS OF STATE

We model the EoSs for the stellar crust and core regions, either separately or self-consistently. For all regions, leptons (electrons and muons) are modeled as a free Fermi gas under the influence of the magnetic field, as they do not interact with respect to the strong force. Nevertheless, nuclei, nucleons (baryon without strangeness, protons and neutrons) and in some cases also hyperons (baryons with net strangeness) are connected with leptons through the conditions of chemical equilibrium and charge neutrality. We do not account for temperature effects in the EoS in this work.

For the microscopic description, we assume the magnetic field B to be (locally) pointing in the z -direction, inducing Landau quantization perpendicular to the magnetic field, in the x - and y -directions. This local “ z ” direction does not directly correspond to any direction in particular within the star; it is merely an abstraction that allows us to calculate the thermodynamic quantities of stellar matter given local values of magnetic field and chemical potentials. We further include the effects of the anomalous magnetic moment (AMM) of the baryons and leptons, creating an asymmetry between the up and down spin states, that either align or anti-align with the local magnetic field, following Ref. (M. Strickland et al. 2012) and references therein.

A.1. *NL3 $\omega\rho$*

The *NL3 $\omega\rho$* model (C. J. Horowitz & J. Piekarewicz 2001a,b; H. Pais & C. Providência 2016) is a relativistic mean-field model of Walecka type with non-linear terms for the mesons, including a term that mixes the vector isoscalar and the vector isovector fields ($\omega\rho$) to model the density dependence of the symmetry energy. It describes bulk matter made of nucleons interacting strongly through the scalar isoscalar meson σ (mediating attraction), the vector isoscalar meson ω (mediating repulsion), and the vector isovector ρ (for isospin asymmetric matter), together with a free gas of electrons and muons. The model reproduces standard nuclear properties for isospin-symmetric matter at saturation: binding energy per baryon $B/A = -16.24$ MeV, saturation density $\rho_0 = 0.148$ fm $^{-3}$, normalized nucleon effective mass $M^*/M = 0.60$, incompressibility $K = 270$ MeV and

symmetry energy $\mathcal{E}_{sym} = 31.66$ MeV with slope $L = 55$ MeV, in addition to being able to describe $2M_\odot$ stars.

A.1.1. Core

Using the same construction as in L. Scurto et al. (2023, 2024) the Lagrangian density of the NL3 $\omega\rho$ model under the influence of magnetic fields is given by

$$\mathcal{L} = \sum_{i=p,n} \mathcal{L}_i + \mathcal{L}_l + \mathcal{L}_\sigma + \mathcal{L}_\omega + \mathcal{L}_\rho + \mathcal{L}_{nl}. \quad (\text{A1})$$

The nucleons and lepton terms are given by

$$\mathcal{L}_i = \bar{\psi}_i [\gamma_\mu iD^\mu - M_* - \frac{1}{2} \kappa_i \sigma_{\mu\nu} F^{\mu\nu}] \psi_i \quad (\text{A2})$$

$$\mathcal{L}_l = \sum_{l=e,\mu} \bar{\psi}_l [\gamma_\mu (i\partial^\mu + eA^\mu) - m_l] \psi_l, \quad (\text{A3})$$

with $i = p, n$ and $l = e, \mu$. κ_i is the AMM coupling (see Tab. 1). m_l is the lepton mass and

$$M_* = M - g_\sigma \phi, \quad (\text{A4})$$

is the nucleon effective mass. The covariant derivative for the nucleons depends on the isoscalar and isovector vector interactions, in addition to the electromagnetic coupling

$$iD^\mu = i\partial^\mu - g_\omega V^\mu - \frac{g_\rho}{2} \boldsymbol{\phi} \cdot \mathbf{b}^\mu - \frac{1 + \tau_3}{2} eA^\mu, \quad (\text{A5})$$

where $e = \sqrt{4\pi/137}$ is the electron charge. The magnetic vector potential is $A^\mu = (0, 0, Bx, 0)$, i.e. B is oriented along the z axis.

The terms for the scalar, vector and isovector mesons are given by

$$\mathcal{L}_\sigma = \frac{1}{2} \left(\partial_\mu \phi \partial^\mu \phi - m_\sigma^2 \phi^2 \right), \quad (\text{A6})$$

$$\mathcal{L}_\omega = -\frac{1}{4} \Omega_{\mu\nu} \Omega^{\mu\nu} + \frac{1}{2} m_\omega^2 V_\mu V^\mu, \quad (\text{A7})$$

$$\mathcal{L}_\rho = -\frac{1}{4} \mathbf{B}_{\mu\nu} \cdot \mathbf{B}^{\mu\nu} + \frac{1}{2} m_\rho^2 \mathbf{b}_\mu \cdot \mathbf{b}^\mu, \quad (\text{A8})$$

with the tensors defined as

$$F_{\mu\nu} = \partial_\mu A_\nu - \partial_\nu A_\mu, \quad (\text{A9})$$

$$\Omega_{\mu\nu} = \partial_\mu V_\nu - \partial_\nu V_\mu, \quad (\text{A10})$$

$$\mathbf{B}_{\mu\nu} = \partial_\mu \mathbf{b}_\nu - \partial_\nu \mathbf{b}_\mu - g_\rho (\mathbf{b}_\mu \times \mathbf{b}_\nu). \quad (\text{A11})$$

The non-linear terms of the interaction read

$$\mathcal{L}_{int} = -\frac{1}{6} \kappa \phi^3 - \frac{1}{24} \lambda \phi^4 + \Lambda_{\omega\rho} g_\omega^2 g_\rho^2 V_\mu V^\mu \mathbf{b}_\mu \cdot \mathbf{b}^\mu. \quad (\text{A12})$$

The neutron density follows

$$\rho_n = \frac{1}{2\pi^2} \sum_s \left[\frac{k_{n,s}^F{}^3}{3} - \frac{1}{2} s \kappa_n B \left(\bar{m}_n k_{n,s}^F + E_n^{F2} \left(\arcsin \left(\frac{\bar{m}_n}{E_n^F} \right) - \frac{\pi}{2} \right) \right) \right], \quad (\text{A13})$$

where the sum is over the spin states, E_n^F is the Fermi energy and the Fermi momentum is given by

$$k_n^{F2} = E_n^{F2} - (M_* - s \kappa_n B)^2. \quad (\text{A14})$$

For the protons and leptons, that interact with the B -field, the density is given by

$$\rho_i = \frac{|q|B}{2\pi^2} \sum_{\nu=0}^{\nu_{\max}^i} \sum_s k_{i,\nu s}^F, \quad (\text{A15})$$

with $i = p, l$, where $\nu = n + \frac{1}{2} - \frac{1}{2} \frac{q}{|q|} s = 0, 1, \dots, \nu_{\max}$ enumerates the Landau levels (LLs) for fermions with electric charge q , ν_{\max} is the largest LL occupied by fully degenerate charged fermions, defined as

$$\nu_{\max}^i = \frac{(E_i^F + s \kappa_i B)^2 - m^2}{2|q|B}, \quad (\text{A16})$$

and the Fermi momentum for charged particles is given by

$$k_{i,\nu s}^{F2} = E_i^{F2} - (\sqrt{m^2 - 2\nu|q|B} - s \kappa_i B)^2, \quad (\text{A17})$$

where for the electrons the AMM is set to zero. The chemical potentials for the protons and neutrons are then given respectively by

$$\mu_p = E_p^F + g_\omega V^0 + \frac{1}{2} g_\rho b^0, \quad (\text{A18})$$

$$\mu_n = E_n^F + g_\omega V^0 - \frac{1}{2} g_\rho b^0. \quad (\text{A19})$$

The total energy density of the magnetized core EoS is given by

$$\mathcal{E} = \mathcal{E}_{kin}^p + \mathcal{E}_{kin}^n + \mathcal{E}_{kin}^l + \mathcal{E}_F, \quad (\text{A20})$$

with \mathcal{E}_F the field contribution written as

$$\mathcal{E}_F = \frac{m_\omega^2}{2} \omega_0^2 + \frac{m_\rho^2}{2} b_{3,0}^2 + \frac{m_\sigma^2}{2} \phi_0^2 + \frac{\kappa}{6} \phi_0^3 + \frac{\lambda}{24} \phi_0^4 + 3\Lambda_{\omega\rho} g_\rho^2 g_\omega^2 \omega_0^2 b_{3,0}^2, \quad (\text{A21})$$

and \mathcal{E}_{kin}^j the single-particle energies of particles $j = p, n, l$

$$\mathcal{E}_{kin}^n = \frac{1}{4\pi^2} \sum_s \left[\frac{1}{3} k_F^n E_n^{F3} - \frac{2}{3} s \kappa_n B E_n^{F3} \left(\arcsin \left(\frac{\bar{m}_n}{E_n^F} \right) - \frac{\pi}{2} \right) - \left(\frac{1}{3} s \kappa_n B + \frac{1}{4} \bar{m}_n \right) \left(\bar{m}_n k_F^n E_n^F + \bar{m}_n^3 \ln \left| \frac{k_F^n + E_n^F}{\bar{m}_n} \right| \right) \right], \quad (\text{A22})$$

$$\mathcal{E}_{kin}^i = \frac{|q|B}{4\pi^2} \sum_{\nu=0}^{\nu_{\max}^i} \sum_s \left[k_{F,\nu s}^i E_i^F + \left(\sqrt{m^2 + 2\nu|q|B} - s\kappa_i B \right)^2 \ln \left| \frac{k_{F,\nu s}^i + E_i^F}{\sqrt{m^2 + 2\nu|q|B} - s\kappa_i B} \right| \right], \quad (\text{A23})$$

with $i = p, l$, where again the AMM of leptons is neglected. The pressure is obtained from the thermodynamic relation

$$P = \mu_p \rho_p + \mu_n \rho_n + \mu_e (\rho_e + \rho_\mu) - \mathcal{E}. \quad (\text{A24})$$

Since the magnetic field induces anisotropy in the energy-momentum tensor, one must calculate the perpendicular component of the pressure. The thermodynamic pressure, Eq. (A24), is equal to the parallel component. The perpendicular component reads:

$$P_{\perp} = P - \mathcal{M}B, \quad (\text{A25})$$

with the magnetization \mathcal{M} given by

$$\mathcal{M} = -\frac{\partial \mathcal{E}}{\partial B}. \quad (\text{A26})$$

A.1.2. Inner crust

In the inner crust, due to the competition between the strong and Coulomb forces, geometrical structures of nucleons are formed, immersed in a sea of neutrons and electrons. We calculate this region of the star from a compressible liquid drop model (CLDM) approximation, where the Gibbs equilibrium conditions are imposed at the intersection between the dense (clusters) and gas (free nucleons). The minimization of the total energy density takes into account the Coulomb and surface terms.

The total energy density of the system in the inner crust is given by:

$$\mathcal{E} = f\mathcal{E}^I + (1-f)\mathcal{E}^{II} + \mathcal{E}_{Coul} + \mathcal{E}_{surf} + \mathcal{E}_e, \quad (\text{A27})$$

where the \mathcal{E} are the bulk energy density of protons and neutrons in the dense (I) and gas (II) phases, calculated using the magnetized NL3 $\omega\rho$ model following Eq. A20, f is the fraction of the heavy cluster in the dense phase, \mathcal{E}_e is the energy density of the electrons, and \mathcal{E}_{Coul} and \mathcal{E}_{surf} are the Coulomb and surface energy density terms, respectively, given by

$$\mathcal{E}_{Coul} = 2\alpha e^2 \pi \Phi R_d^2 (\rho_p^I - \rho_p^{II})^2, \quad (\text{A28})$$

$$\mathcal{E}_{surf} = \frac{\sigma \alpha D}{R_d}, \quad (\text{A29})$$

with

$$\begin{aligned} \Phi &= \left(\frac{2 - D\alpha^{1-2/D}}{D-2} + \alpha \right) \frac{1}{D+2}, & D = 1, 3, \\ \Phi &= \frac{\alpha - 1 - \ln \alpha}{D+2}, & D = 2, \end{aligned} \quad (\text{A30})$$

where D is the dimension of the geometry, $\alpha = f$ for droplets, rods and slabs, and $\alpha = 1 - f$ for bubbles and tubes, and σ is the surface tension functional, that is calculated from a fit to a Thomas-Fermi calculation (S. S. Avancini et al. 2012). From the minimization of Eq. (A27), we obtain the following relation between the surface and the Coulomb corrections, the expression for the radius of the cluster

$$\mathcal{E}_{surf} = 2\mathcal{E}_{Coul}, \quad (\text{A31})$$

$$R_d = \left[\frac{\sigma D}{4\pi e^2 \Phi (\rho_p^I - \rho_p^{II})^2} \right]^{1/3}, \quad (\text{A32})$$

and the Gibbs equilibrium, given by

$$\mu_n^I = \mu_n^{II}, \quad (\text{A33})$$

$$\mu_p^I = \mu_p^{II} - \frac{\mathcal{E}_{surf}}{(1-f)f(\rho_p^I - \rho_p^{II})}, \quad (\text{A34})$$

$$P^I = P^{II} \quad (\text{A35})$$

$$+ \mathcal{E}_{surf} \left[\frac{3}{2\alpha} \frac{\partial \alpha}{\partial f} + \frac{1}{2\Phi} \frac{\partial \Phi}{\partial f} - \frac{((1-f)\rho_p^I + f\rho_p^{II})}{(1-f)f(\rho_p^I - \rho_p^{II})} \right]. \quad (\text{A36})$$

For further details, the reader can consult L. Scurto et al. (2023). As mentioned in Sec. 2, this description for the inner crust of neutron stars is combined with the SLy4 EoS for the outer crust (F. Douchin & P. Haensel 2001).

A.2. CMF

To describe bulk matter interacting with respect to the strong force, but more realistically describing large density, we make use of the Chiral Mean Field (CMF) model. It is a relativistic microscopic model that describes nucleons, hyperons, and quarks interacting strongly through scalar mesons (mediating attraction) and vector mesons (mediating repulsion), together with a free gas of electrons and muons (V. Dexheimer & S. Schramm 2008). Most importantly, the model reproduces the chiral symmetry restoration phase transition and the deconfinement phase transition to quark matter V. A. Dexheimer & S. Schramm (2010), two important features of Quantum Chromodynamics (QCD), in the high-energy regime. In this work, we do not include finite-temperature effects in the EoS, so high energy means high baryon chemical potential μ_B , related (in a complex way that depends on the EoS) to the baryon number density n_B .

The CMF model is based on a nonlinear realization of the chiral linear sigma model (P. Papazoglou et al. 1998). Like other relativistic mean-field (RMF) models, it uses mean-field mesons to approximate the effects of gluons,

simplifying considerably the calculations of QCD. On the other hand, chiral models differ from RMF Walecka-type models, as they have particle masses generated by the medium. In this work, we do not include quarks in order to disentangle the effects of magnetic field and deconfinement. See Ref. (J. Peterson et al. 2023) for a discussion on how magnetic fields and temperature affect the dense-matter EoS described by chiral models with quarks. The model reproduces standard nuclear properties for isospin-symmetric matter at saturation: binding energy per baryon $B/A = -16$ MeV, saturation density $\rho_0 = 0.15 \text{ fm}^{-3}$, incompressibility $K = 300$ MeV and symmetry energy $\mathcal{E}_{sym} = 30$ MeV with slope $L = 88$ MeV, in addition to being able to describe $2M_\odot$ stars (see Ref. V. Dexheimer et al. (2019) for a version of CMF with $\omega\rho$ interaction, but no magnetic field effects).

The CMF Lagrangian density, following the CMF formalism with magnetic-field effects presented in (V. Dexheimer et al. 2012) is

$$\mathcal{L} = \mathcal{L}_{kin} + \mathcal{L}_{int} + \mathcal{L}_{scal} + \mathcal{L}_{vec} + \mathcal{L}_{esb}, \quad (\text{A37})$$

where the kinetic energy term for baryons is

$$\mathcal{L}_{kin} = \sum_{i \in B} \left(\bar{\psi}_i i \left(\gamma_\mu \partial^\mu + \frac{1}{2} \kappa_i \sigma^{\mu\nu} F_{\mu\nu} \right) \psi_i \right), \quad (\text{A38})$$

the baryon-meson interaction term is

$$\mathcal{L}_{int} = - \sum_{i \in B} \left(\bar{\psi}_i [\gamma_0 (g_{i\omega}\omega + g_{i\rho}\rho + g_{i\phi}\phi) + m_i^*] \psi_i \right), \quad (\text{A39})$$

the scalar meson self-interaction term is

$$\begin{aligned} \mathcal{L}_{scal} = & -\frac{1}{2} k_0 \chi_0^2 (\sigma^2 + \delta^2 + \zeta^2) + k_1 (\sigma^2 + \delta^2 + \zeta^2)^2 \\ & + k_2 \left(\frac{\sigma^4 + \delta^4}{2} + \zeta^4 + 3(\sigma\delta)^2 \right) + k_3 \chi_0 (\sigma^2 - \delta^2) \zeta \\ & - k_4 \chi_0^4 + \frac{\epsilon}{3} \chi_0^4 \ln \left(\frac{(\sigma^2 - \delta^2) \zeta}{\sigma_0^2 \zeta_0} \right), \end{aligned} \quad (\text{A40})$$

the vector meson self-interaction term is

$$\begin{aligned} \mathcal{L}_{vec} = & \frac{1}{2} (m_\omega^2 \omega^2 + m_\rho^2 \rho^2 + m_\phi^2 \phi^2) \\ & + g_4 \left(\omega^4 + \frac{\phi^4}{4} + 3\omega^2 \phi^2 + \frac{4\omega^3 \phi}{\sqrt{2}} + \frac{2\omega \phi^3}{\sqrt{2}} \right), \end{aligned} \quad (\text{A41})$$

and the term corresponding to an explicit breaking of chiral symmetry is

$$\mathcal{L}_{esb} = - \left(m_\pi^2 f_\pi \sigma + (\sqrt{2} m_k^2 f_k - \frac{1}{\sqrt{2}} m_\pi^2 f_\pi) \zeta \right), \quad (\text{A42})$$

in addition to a constant term. In these expressions ψ_i is the baryon or lepton wave function, γ_μ represents the Dirac matrices, σ , δ , and ζ are scalar mesons, while ω , ρ , and ϕ are the vector mesons; g_{ij} are coupling constants between baryons i and mesons j (see Tables in Ref. N. Cruz-Camacho et al. (2024) for coupling values and additional details). Furthermore, m_i^* is the effective mass of baryon i , $\sigma^{\mu\nu} = \frac{i}{2} [\gamma^\mu, \gamma^\nu]$, and $F^{\mu\nu}$ is the electromagnetic tensor. The AMM couplings κ_i are shown in Tab. 1.

The Lagrangian density cannot be fully decoupled between baryons and mesons. Instead, the result is a relativistic Fermi gas with an effective mass generated by the scalar meson fields $m_i^* = g_{i\sigma}\sigma + g_{i\delta}\delta + g_{i\zeta}\zeta + \Delta m_i^{**}$ and effective Fermi energy modified by the vector meson fields $E_i^* = E_i - g_{i\omega}\omega - g_{i\rho}\rho - g_{i\phi}\phi$. At $T = 0$, the Fermi energy of particles corresponds to their chemical potentials $E_i \rightarrow \mu_i = B_i \mu_B + Q_i \mu_Q$, where B_i is the particle baryon number (1 for baryons and 0 for leptons), Q_i the particle electric charge, μ_B the baryon chemical potential, and μ_Q the charge chemical potential. While μ_B is our independent variable, μ_Q is determined by imposing charge neutrality and chemical equilibrium with leptons. The mass term is obtained for leptons from Eq. A39 setting $g_i = 0$, $m_i^* = m_i$, in addition to $\mu_i^* = \mu_i$.

Additionally, \bar{m} is the particle effective mass modified by the magnetic field given by $\bar{m}_i = \sqrt{m_i^{*2} + 2\nu|q_i|B - s\kappa_i B}$ for charged particles and $\bar{m}_i = m_i^* - s\kappa_i B$ for uncharged particles, $\nu = n + \frac{1}{2} - \frac{s}{2} \frac{q_i}{|q_i|}$ is the Landau level, with n being the discretized orbital angular momentum of the particle in the transverse plane, and $s = \pm 1$ the spin projection of the particle along the direction of the magnetic field.

From here, we obtain the expressions for number density, scalar density, energy density, parallel pressure (z-direction), and perpendicular pressure (x- and y- directions) of charged particles (M. Strickland et al. 2012):

$$n_i = \frac{|q_i|B}{2\pi^2} \sum_{s=\pm 1} \sum_{\nu \leq \nu_{max}} k_{z_i}, \quad (\text{A43})$$

$$n_{S,i} = \frac{|q_i|B}{2\pi^2} \frac{\bar{m}_i m_i^*}{\bar{m}_i + s_i \kappa_i B} \ln \left(\frac{\sqrt{k_{z_i}^2 + \mu_i^*}}{\bar{m}_i} \right), \quad (\text{A44})$$

** Δm_i is the bare mass, which does not come from the mean fields. It has values 150 MeV for nucleons and 342.3 MeV for hyperons.

Table 1. Table of AMM coupling strengths for leptons and baryons (P. A. Zyla et al. 2020). κ_i is equal to the product of the AMM coupling \mathcal{K}_i and an appropriate magneton. For baryons, this is the nuclear magneton $\frac{e}{2m_p}$, whereas, for leptons the magneton is $\frac{e}{2m_i}$, yielding unique values for the electron and muon. In the magneton expressions, e is the elementary charge and the masses are the vacuum masses.

	i	e	μ	p	n	Λ	Σ^+	Σ^0	Σ^-	Ξ^0	Ξ^-
	\mathcal{K}_i	0.00116	0.001166	1.79	-1.91	-0.61	1.67	1.61	-0.38	-1.25	0.06

$$\varepsilon_i = \frac{|q_i|B}{4\pi^2} \sum_{s=\pm 1} \sum_{\nu \leq \nu_{max}} \left[\mu_i^* k_{z_i} + \bar{m}_i^2 \ln \left(\frac{\mu_i^* + k_{z_i}}{\bar{m}_i} \right) \right], \quad (\text{A45})$$

$$P_{\parallel i} = \frac{|q_i|B}{4\pi^2} \sum_{s=\pm 1} \sum_{\nu \leq \nu_{max}} \left[\mu_i^* k_{z_i} - \bar{m}_i^2 \ln \left(\frac{\mu_i^* + k_{z_i}}{\bar{m}_i} \right) \right], \quad (\text{A46})$$

$$P_{\perp i} = \frac{|q_i|B^2}{2\pi^2} \sum_{s=\pm 1} \sum_{\nu \leq \nu_{max}} \left[\left(\frac{|q_i| \nu \bar{m}_i}{\sqrt{m_i^{*2} + 2\nu|q_i|B}} - s\kappa_i \bar{m}_i \right) \ln \left(\frac{\mu_i^* + k_{z_i}}{\bar{m}_i} \right) \right], \quad (\text{A47})$$

where the Fermi momentum of particle i in the local magnetic-field direction is $k_{z_i} = \sqrt{\mu_i^{*2} - \bar{m}_i^2}$ and $\nu_{max} = \left\lfloor \frac{(\mu_i^* + s\kappa_i B)^2 - m_i^{*2}}{2|q_i|B} \right\rfloor$ is the largest Landau level for which k_{z_i} is real. For uncharged particles, these equations are instead

$$n_i = \frac{1}{2\pi^2} \sum_{s=\pm 1} \left[\frac{k_i^3}{3} - \frac{s\kappa_i B}{2} \left(m_i^* k_i \mu_i^{*2} \left(\arcsin \left(\frac{m_i^*}{\mu_i^*} \right) - \frac{\pi}{2} \right) \right) \right], \quad (\text{A48})$$

$$n_{S,i} = \frac{1}{2\pi^2} m_i^* \left(\frac{k_i \mu_i^*}{2} - \frac{(m_i^* - s\kappa_i B)^2}{2} \times \ln \left(\frac{k_i + \mu_i^*}{m_i^* - s\kappa_i B} \right) \right), \quad (\text{A49})$$

$$\varepsilon_i = \frac{1}{48\pi^2} \sum_{s=\pm 1} \left[\mu_i^* k_i \left(6\mu_i^{*2} - 3\bar{m}_i^2 - 4s\kappa_i B \bar{m}_i \right) - 8s\kappa_i B \mu_i^{*3} \left(\arcsin \left(\frac{m_i^*}{\mu_i^*} \right) - \frac{\pi}{2} \right) - \bar{m}_i^3 (3\bar{m}_i + 4s\kappa_i B) \ln \left(\frac{\mu_i^* + k_i}{\bar{m}_i} \right) \right],$$

$$P_{\parallel i} = \frac{1}{48\pi^2} \sum_{s=\pm 1} \left[\mu_i^* k_i \left(2\mu_i^{*2} - 5\bar{m}_i^2 - 8s\kappa_i B \bar{m}_i \right) - 4s\kappa_i B \mu_i^{*3} \left(\arcsin \left(\frac{m_i^*}{\mu_i^*} \right) - \frac{\pi}{2} \right) + \bar{m}_i^3 (3\bar{m}_i + 4s\kappa_i B) \ln \left(\frac{\mu_i^* + k_i}{\bar{m}_i} \right) \right], \quad (\text{A50})$$

$$P_{\perp i} = \frac{1}{48\pi^2} \sum_{s=\pm 1} \left[\mu_i^* k_F (2\mu_i^{*2} - 5\bar{m}^2 - 12s\kappa_i B \bar{m} - 12(s\kappa_i B)^2) + 3\bar{m}^2 (\bar{m} + 2s\kappa_i B)^2 \ln \left(\frac{\mu_i^* + k_F}{\bar{m}} \right) \right]. \quad (\text{A51})$$

where the parallel and perpendicular pressures specify the components of the energy-momentum tensor of matter in the local rest frame of the system. The total baryon number density is then the sum over all particle number densities multiplied by their baryon number B_i , $n_B = \sum_i B_i n_i$. In addition to a sum over particles, matter energy density and pressures receive additional terms from the mesons (with the vacuum subtracted) and free leptons. At $T = 0$, mesons provide no contribution to the kinetic term, so their contributions are simply $\mathcal{L}_{\text{mesons}} = \mathcal{L}_{\text{scal}} + \mathcal{L}_{\text{vec}} + \mathcal{L}_{\text{esb}} - \mathcal{L}_{\text{vacuum}}$. The total energy density, parallel pressure, and perpendicular pressure then become

$$\varepsilon = \sum_{i \in B, \text{lep}} \varepsilon_i + \varepsilon_{\text{int}} - \mathcal{L}_{\text{mesons}}, \quad (\text{A52})$$

$$P_{\parallel} = \sum_{i \in B, \text{lep}} P_i + \mathcal{L}_{\text{mesons}}, \quad (\text{A53})$$

$$P_{\perp} = \sum_{i \in B, \text{lep}} P_i + \mathcal{L}_{\text{mesons}}, \quad (\text{A54})$$

with $\varepsilon_{\text{int}} = \sum_{i \in B} (g_{i\omega}\omega + g_{i\phi}\phi + g_{i\rho}\rho) n_i$.

In Fig. A.1 we compare these two EoS, which differ in the core and inner crust region. The outer core was smoothly transitioned to SLy4 (F. Douchin & P. Haensel 2001). We show the thermodynamic pressure as function of the density for a value of the magnetic field of 10^{16} G. Even though NL3 $\omega\rho$ has a smaller L at saturation density, it becomes stiffer than CMF because this one includes exotic degrees of freedom. The CMF

presents a first-order phase transition at very low densities, reminiscent of the nuclear liquid-gas phase transition for isospin symmetric matter.

B. PRIMITIVE INVERSION SCHEME

One conceptual challenge arises in the use of standard primitive inversion algorithms, since the EoS now acquires a velocity dependence through the use of the comoving magnetic field strength, b . In other words, the equations acquire a fluid frame dependence that needs to be accounted for. Rather than modifying the algorithm (W. Kastaun et al. 2021) itself, we make use of the fact that the anisotropic pressure corrections are intrinsically small ($< 10\%$). While this overall leads to a significant increase in computational cost, it is sufficient for a first exploration of this effect.

We call $Y_B = \sqrt{b_\mu b^\mu}$ the effective magnetic field composition variable, such that the EoS we use is given by

$$\tilde{P} = \tilde{P}_B(\rho, Y_B) + \rho\varepsilon(\Gamma_{\text{th}} - 1), \quad (\text{B55})$$

where the second term has been added to approximately capture thermal effects (A. Bauswein et al. 2010). We nominally choose $\Gamma_{\text{th}} = 1.8$.

Our modified scheme operates as follows:

1. Choose an initial guess $Y_B = B$, and set the magnetic field $\bar{B}^i = B^i$ to be used in the next step.
2. Solve the primitive inversion (W. Kastaun et al. 2021) for fixed Y_B , and obtain an approximate value, \bar{v}^i , for the velocity.
3. Recompute $\bar{Y}_B = \sqrt{\bar{b}^2}$, where $\bar{b}^2 = \frac{B^2}{\bar{W}^2} + (B^i \bar{v}_i)^2$ is the comoving magnetic field strength, and $\bar{W}^{-1} = \sqrt{1 - \bar{v}_i \bar{v}^i}$ is the inverse Lorentz factor, both computed from \bar{v}^i .
4. Using the approximate compositional value of \bar{Y}_B , compute the polarization $\bar{\kappa}$, and use it to rescale the magnetic field $\bar{B}^i = \sqrt{1 - \bar{\kappa}} B^i$.
5. Iterate steps 2.-4. until convergence in \bar{Y}_B , which empirically takes about five iterations in regions of high magnetization.

REFERENCES

- Abbott, B. P., et al. 2017, Phys. Rev. Lett., 119, 161101, doi: [10.1103/PhysRevLett.119.161101](https://doi.org/10.1103/PhysRevLett.119.161101)
- Abbott, B. P., et al. 2018, Phys. Rev. Lett., 121, 161101, doi: [10.1103/PhysRevLett.121.161101](https://doi.org/10.1103/PhysRevLett.121.161101)
- Abbott, B. P., et al. 2020, Astrophys. J. Lett., 892, L3, doi: [10.3847/2041-8213/ab75f5](https://doi.org/10.3847/2041-8213/ab75f5)
- Aguilera-Miret, R., Palenzuela, C., Carrasco, F., & Viganò, D. 2023, Phys. Rev. D, 108, 103001, doi: [10.1103/PhysRevD.108.103001](https://doi.org/10.1103/PhysRevD.108.103001)
- Aguilera-Miret, R., Viganò, D., & Palenzuela, C. 2022, Astrophys. J. Lett., 926, L31, doi: [10.3847/2041-8213/ac50a7](https://doi.org/10.3847/2041-8213/ac50a7)
- Aguirre, R., & Bauer, E. 2015, J. Phys. G, 42, 105101, doi: [10.1088/0954-3899/42/10/105101](https://doi.org/10.1088/0954-3899/42/10/105101)
- Aguirre, R., Bauer, E., & Vidana, I. 2014, Phys. Rev. C, 89, 035809, doi: [10.1103/PhysRevC.89.035809](https://doi.org/10.1103/PhysRevC.89.035809)
- Alcubierre, M., Bruegmann, B., Diener, P., et al. 2003, Phys. Rev. D, 67, 084023, doi: [10.1103/PhysRevD.67.084023](https://doi.org/10.1103/PhysRevD.67.084023)
- Alford, M. G., Bovard, L., Hanauske, M., Rezzolla, L., & Schwenzer, K. 2018, Phys. Rev. Lett., 120, 041101, doi: [10.1103/PhysRevLett.120.041101](https://doi.org/10.1103/PhysRevLett.120.041101)
- Andersen, B. C., et al. 2020, Nature, 587, 54, doi: [10.1038/s41586-020-2863-y](https://doi.org/10.1038/s41586-020-2863-y)
- Anderson, M., Hirschmann, E. W., Lehner, L., et al. 2008, Phys. Rev. Lett., 100, 191101, doi: [10.1103/PhysRevLett.100.191101](https://doi.org/10.1103/PhysRevLett.100.191101)
- Annala, E., Gorda, T., Kurkela, A., & Vuorinen, A. 2018, Phys. Rev. Lett., 120, 172703, doi: [10.1103/PhysRevLett.120.172703](https://doi.org/10.1103/PhysRevLett.120.172703)
- Avancini, S., Bertolino, B. P., Rabhi, A., et al. 2018, Phys. Rev. C, 98, 025805, doi: [10.1103/PhysRevC.98.025805](https://doi.org/10.1103/PhysRevC.98.025805)
- Avancini, S. S., Barros, C. C., Brito, L., et al. 2012, Phys. Rev. C, 85, 035806, doi: [10.1103/PhysRevC.85.035806](https://doi.org/10.1103/PhysRevC.85.035806)
- Backes, B. C. T., Marquez, K. D., & Menezes, D. P. 2021, Eur. Phys. J. A, 57, 229, doi: [10.1140/epja/s10050-021-00544-2](https://doi.org/10.1140/epja/s10050-021-00544-2)
- Baiotti, L., Giacomazzo, B., & Rezzolla, L. 2008, Phys. Rev. D, 78, 084033, doi: [10.1103/PhysRevD.78.084033](https://doi.org/10.1103/PhysRevD.78.084033)
- Bamber, J., Tsokaros, A., Ruiz, M., & Shapiro, S. L. 2024, Phys. Rev. D, 110, 024046, doi: [10.1103/PhysRevD.110.024046](https://doi.org/10.1103/PhysRevD.110.024046)
- Bamber, J., Tsokaros, A., Ruiz, M., & Shapiro, S. L. 2025, Phys. Rev. D, 111, 044038, doi: [10.1103/PhysRevD.111.044038](https://doi.org/10.1103/PhysRevD.111.044038)
- Bao, S. S., Hu, J. N., Zhang, Z. W., & Shen, H. 2014, Phys. Rev. C, 90, 045802, doi: [10.1103/PhysRevC.90.045802](https://doi.org/10.1103/PhysRevC.90.045802)

- Barrère, P., Guilet, J., Reboul-Salze, A., Raynaud, R., & Janka, H. T. 2022, *Astron. Astrophys.*, 668, A79, doi: [10.1051/0004-6361/202244172](https://doi.org/10.1051/0004-6361/202244172)
- Baumgarte, T. W., & Shapiro, S. L. 2003, *Astrophys. J.*, 585, 921, doi: [10.1086/346103](https://doi.org/10.1086/346103)
- Bauswein, A., Janka, H. T., & Oechslin, R. 2010, *Phys. Rev. D*, 82, 084043, doi: [10.1103/PhysRevD.82.084043](https://doi.org/10.1103/PhysRevD.82.084043)
- Bauswein, A., Just, O., Janka, H.-T., & Stergioulas, N. 2017, *Astrophys. J. Lett.*, 850, L34, doi: [10.3847/2041-8213/aa9994](https://doi.org/10.3847/2041-8213/aa9994)
- Baym, G., Bethe, H. A., & Pethick, C. 1971, *Nucl. Phys. A*, 175, 225, doi: [10.1016/0375-9474\(71\)90281-8](https://doi.org/10.1016/0375-9474(71)90281-8)
- Bejger, M., Blaschke, D., Haensel, P., Zdunik, J. L., & Fortin, M. 2017, *Astron. Astrophys.*, 600, A39, doi: [10.1051/0004-6361/201629580](https://doi.org/10.1051/0004-6361/201629580)
- Benvenuto, O. G., Bauer, E., & Vidaña, I. 2023, *Eur. Phys. J. A*, 59, 159, doi: [10.1140/epja/s10050-023-01070-z](https://doi.org/10.1140/epja/s10050-023-01070-z)
- Bernuzzi, S., & Hilditch, D. 2010, *Phys. Rev. D*, 81, 084003, doi: [10.1103/PhysRevD.81.084003](https://doi.org/10.1103/PhysRevD.81.084003)
- Bochenek, C. D., Ravi, V., Belov, K. V., et al. 2020, *Nature*, 587, 59, doi: [10.1038/s41586-020-2872-x](https://doi.org/10.1038/s41586-020-2872-x)
- Boss, A. P., & Keiser, S. A. 2013, *ApJ*, 764, 136, doi: [10.1088/0004-637X/764/2/136](https://doi.org/10.1088/0004-637X/764/2/136)
- Bozzola, G. 2021, *The Journal of Open Source Software*, 6, 3099, doi: [10.21105/joss.03099](https://doi.org/10.21105/joss.03099)
- Bransgrove, A., Beloborodov, A. M., & Levin, Y. 2020, doi: [10.3847/1538-4357/ab93b7](https://doi.org/10.3847/1538-4357/ab93b7)
- Bransgrove, A., Levin, Y., & Beloborodov, A. 2018, *Mon. Not. Roy. Astron. Soc.*, 473, 2771, doi: [10.1093/mnras/stx2508](https://doi.org/10.1093/mnras/stx2508)
- Bucciantini, N., & Del Zanna, L. 2013, *Mon. Not. Roy. Astron. Soc.*, 428, 71, doi: [10.1093/mnras/sts005](https://doi.org/10.1093/mnras/sts005)
- Chabanov, M., Tootle, S. D., Most, E. R., & Rezzolla, L. 2023, *Astrophys. J. Lett.*, 945, L14, doi: [10.3847/2041-8213/acbbc5](https://doi.org/10.3847/2041-8213/acbbc5)
- Chamel, N., Stoyanov, Z. K., Mihailov, L. M., et al. 2015, *Phys. Rev. C*, 91, 065801, doi: [10.1103/PhysRevC.91.065801](https://doi.org/10.1103/PhysRevC.91.065801)
- Chandra, M., Gammie, C. F., Foucart, F., & Quataert, E. 2015, *Astrophys. J.*, 810, 162, doi: [10.1088/0004-637X/810/2/162](https://doi.org/10.1088/0004-637X/810/2/162)
- Chatterjee, D., Elghozi, T., Novak, J., & Oertel, M. 2015, *Mon. Not. Roy. Astron. Soc.*, 447, 3785, doi: [10.1093/mnras/stu2706](https://doi.org/10.1093/mnras/stu2706)
- Chatterjee, D., Gulminelli, F., & Menezes, D. P. 2019, *JCAP*, 03, 035, doi: [10.1088/1475-7516/2019/03/035](https://doi.org/10.1088/1475-7516/2019/03/035)
- Chatziioannou, K., Haster, C.-J., & Zimmerman, A. 2018, *Phys. Rev. D*, 97, 104036, doi: [10.1103/PhysRevD.97.104036](https://doi.org/10.1103/PhysRevD.97.104036)
- Chu, P.-C., Wang, X., Chen, L.-W., & Huang, M. 2015, *Phys. Rev. D*, 91, 023003, doi: [10.1103/PhysRevD.91.023003](https://doi.org/10.1103/PhysRevD.91.023003)
- Cioffi, R., Kastaun, W., Giacomazzo, B., et al. 2017, *Phys. Rev. D*, 95, 063016, doi: [10.1103/PhysRevD.95.063016](https://doi.org/10.1103/PhysRevD.95.063016)
- Combi, L., & Siegel, D. M. 2023a, *Astrophys. J.*, 944, 28, doi: [10.3847/1538-4357/acac29](https://doi.org/10.3847/1538-4357/acac29)
- Combi, L., & Siegel, D. M. 2023b, *Phys. Rev. Lett.*, 131, 231402, doi: [10.1103/PhysRevLett.131.231402](https://doi.org/10.1103/PhysRevLett.131.231402)
- Cruz-Camacho, N., Kumar, R., Reinke Pelicer, M., et al. 2024, Phase Stability in the 3-Dimensional Open-source Code for the Chiral mean-field Model, <https://arxiv.org/abs/2409.06837>
- Curtis, S., Bosch, P., Mösta, P., et al. 2024, *Astrophys. J. Lett.*, 961, L26, doi: [10.3847/2041-8213/ad0fe1](https://doi.org/10.3847/2041-8213/ad0fe1)
- De Haas, W. J., & Van Alphen, P. M. 1930, *Proc. Acad. Sci. Amst.*, 33, 1106. <https://www.dwc.knaw.nl/DL/publications/PU00015989.pdf>
- Del Zanna, L., Zanotti, O., Bucciantini, N., & Londrillo, P. 2007, *Astron. Astrophys.*, 473, 11, doi: [10.1051/0004-6361:20077093](https://doi.org/10.1051/0004-6361:20077093)
- Dexheimer, V., de Oliveira Gomes, R., Schramm, S., & Pais, H. 2019, *J. Phys. G*, 46, 034002, doi: [10.1088/1361-6471/ab01f0](https://doi.org/10.1088/1361-6471/ab01f0)
- Dexheimer, V., Franzon, B., Gomes, R. O., et al. 2017, *Phys. Lett. B*, 773, 487, doi: [10.1016/j.physletb.2017.09.008](https://doi.org/10.1016/j.physletb.2017.09.008)
- Dexheimer, V., Negreiros, R., & Schramm, S. 2012, *Eur. Phys. J. A*, 48, 189, doi: [10.1140/epja/i2012-12189-y](https://doi.org/10.1140/epja/i2012-12189-y)
- Dexheimer, V., & Schramm, S. 2008, *Astrophys. J.*, 683, 943, doi: [10.1086/589735](https://doi.org/10.1086/589735)
- Dexheimer, V. A., & Schramm, S. 2010, *Phys. Rev. C*, 81, 045201, doi: [10.1103/PhysRevC.81.045201](https://doi.org/10.1103/PhysRevC.81.045201)
- Douchin, F., & Haensel, P. 2001, *Astron. Astrophys.*, 380, 151, doi: [10.1051/0004-6361:20011402](https://doi.org/10.1051/0004-6361:20011402)
- Duez, M. D., Liu, Y. T., Shapiro, S. L., & Stephens, B. C. 2005, *Phys. Rev. D*, 72, 024028, doi: [10.1103/PhysRevD.72.024028](https://doi.org/10.1103/PhysRevD.72.024028)
- Endrizzi, A., Cioffi, R., Giacomazzo, B., Kastaun, W., & Kawamura, T. 2016, *Class. Quant. Grav.*, 33, 164001, doi: [10.1088/0264-9381/33/16/164001](https://doi.org/10.1088/0264-9381/33/16/164001)
- Espino, P. L., Hammond, P., Radice, D., et al. 2024, *Phys. Rev. Lett.*, 132, 211001, doi: [10.1103/PhysRevLett.132.211001](https://doi.org/10.1103/PhysRevLett.132.211001)
- Etienne, Z. B., Paschalidis, V., Haas, R., Mösta, P., & Shapiro, S. L. 2015, *Class. Quant. Grav.*, 32, 175009, doi: [10.1088/0264-9381/32/17/175009](https://doi.org/10.1088/0264-9381/32/17/175009)
- Fang, J., Avancini, S., Pais, H., & Providência, C. 2016, *Phys. Rev. C*, 94, 062801, doi: [10.1103/PhysRevC.94.062801](https://doi.org/10.1103/PhysRevC.94.062801)

- Fang, J., Pais, H., Pratapsi, S., et al. 2017a, *Phys. Rev. C*, 95, 045802, doi: [10.1103/PhysRevC.95.045802](https://doi.org/10.1103/PhysRevC.95.045802)
- Fang, J., Pais, H., Pratapsi, S., & Providência, C. 2017b, *Phys. Rev. C*, 95, 062801, doi: [10.1103/PhysRevC.95.062801](https://doi.org/10.1103/PhysRevC.95.062801)
- Fattoyev, F. J., Horowitz, C. J., Piekarewicz, J., & Reed, B. 2020, *Phys. Rev. C*, 102, 065805, doi: [10.1103/PhysRevC.102.065805](https://doi.org/10.1103/PhysRevC.102.065805)
- Ferrer, E. J., de la Incera, V., Keith, J. P., Portillo, I., & Springsteen, P. L. 2010, *Phys. Rev. C*, 82, 065802, doi: [10.1103/PhysRevC.82.065802](https://doi.org/10.1103/PhysRevC.82.065802)
- Ferrer, E. J., & Hackebill, A. 2022, *Int. J. Mod. Phys. A*, 37, 2250048, doi: [10.1142/S0217751X22500488](https://doi.org/10.1142/S0217751X22500488)
- Fields, J., Prakash, A., Breschi, M., et al. 2023, *Astrophys. J. Lett.*, 952, L36, doi: [10.3847/2041-8213/ace5b2](https://doi.org/10.3847/2041-8213/ace5b2)
- Figura, A., Lu, J. J., Burgio, G. F., Li, Z. H., & Schulze, H. J. 2020, *Phys. Rev. D*, 102, 043006, doi: [10.1103/PhysRevD.102.043006](https://doi.org/10.1103/PhysRevD.102.043006)
- Fogaça, D. A., Sanches, S. M., Motta, T. F., & Navarra, F. S. 2016, *Phys. Rev. C*, 94, 055805, doi: [10.1103/PhysRevC.94.055805](https://doi.org/10.1103/PhysRevC.94.055805)
- Fraga, E. S., & Mizher, A. J. 2008, *Phys. Rev. D*, 78, 025016, doi: [10.1103/PhysRevD.78.025016](https://doi.org/10.1103/PhysRevD.78.025016)
- Franzon, B., Dexheimer, V., & Schramm, S. 2016, *Mon. Not. Roy. Astron. Soc.*, 456, 2937, doi: [10.1093/mnras/stv2606](https://doi.org/10.1093/mnras/stv2606)
- Gavassino, L., & Noronha, J. 2024, *Phys. Rev. D*, 109, 096040, doi: [10.1103/PhysRevD.109.096040](https://doi.org/10.1103/PhysRevD.109.096040)
- Giacomazzo, B., & Perna, R. 2013, *Astrophys. J. Lett.*, 771, L26, doi: [10.1088/2041-8205/771/2/L26](https://doi.org/10.1088/2041-8205/771/2/L26)
- Giacomazzo, B., Rezzolla, L., & Baiotti, L. 2011, *Phys. Rev. D*, 83, 044014, doi: [10.1103/PhysRevD.83.044014](https://doi.org/10.1103/PhysRevD.83.044014)
- Giacomazzo, B., Zrake, J., Duffell, P., MacFadyen, A. I., & Perna, R. 2015, *Astrophys. J.*, 809, 39, doi: [10.1088/0004-637X/809/1/39](https://doi.org/10.1088/0004-637X/809/1/39)
- Gomes, R. O., Pais, H., Dexheimer, V., Providência, C., & Schramm, S. 2019, *Astron. Astrophys.*, 627, A61, doi: [10.1051/0004-6361/201935310](https://doi.org/10.1051/0004-6361/201935310)
- Gorbar, E. V., Miransky, V. A., & Shovkovy, I. A. 2011, *Phys. Rev. D*, 83, 085003, doi: [10.1103/PhysRevD.83.085003](https://doi.org/10.1103/PhysRevD.83.085003)
- Gourgoulhon, E. 2007, 3+1 formalism and bases of numerical relativity, <https://arxiv.org/abs/gr-qc/0703035>
- Grandclement, P. 2010, *J. Comput. Phys.*, 229, 3334, doi: [10.1016/j.jcp.2010.01.005](https://doi.org/10.1016/j.jcp.2010.01.005)
- Gutiérrez, E. M., Cook, W., Radice, D., et al. 2025, <https://arxiv.org/abs/2506.18995>
- Haber, A., Preis, F., & Schmitt, A. 2016, *AIP Conf. Proc.*, 1701, 080010, doi: [10.1063/1.4938699](https://doi.org/10.1063/1.4938699)
- Hanauske, M., Takami, K., Bovard, L., et al. 2017, *Phys. Rev. D*, 96, 043004, doi: [10.1103/PhysRevD.96.043004](https://doi.org/10.1103/PhysRevD.96.043004)
- Harris, C. R., Millman, K. J., van der Walt, S. J., et al. 2020, *Nature*, 585, 357, doi: [10.1038/s41586-020-2649-2](https://doi.org/10.1038/s41586-020-2649-2)
- Harutyunyan, A., Nathanail, A., Rezzolla, L., & Sedrakian, A. 2018, *Eur. Phys. J. A*, 54, 191, doi: [10.1140/epja/i2018-12624-1](https://doi.org/10.1140/epja/i2018-12624-1)
- Hilditch, D., Bernuzzi, S., Thierfelder, M., et al. 2013, *Phys. Rev. D*, 88, 084057, doi: [10.1103/PhysRevD.88.084057](https://doi.org/10.1103/PhysRevD.88.084057)
- Horowitz, C. J., & Piekarewicz, J. 2001a, *Phys. Rev. Lett.*, 86, 5647, doi: [10.1103/PhysRevLett.86.5647](https://doi.org/10.1103/PhysRevLett.86.5647)
- Horowitz, C. J., & Piekarewicz, J. 2001b, *Phys. Rev. C*, 64, 062802, doi: [10.1103/PhysRevC.64.062802](https://doi.org/10.1103/PhysRevC.64.062802)
- Hunter, J. D. 2007, *Computing in Science & Engineering*, 9, 90, doi: [10.1109/MCSE.2007.55](https://doi.org/10.1109/MCSE.2007.55)
- Igoshev, A., Barrère, P., Raynaud, R., et al. 2025, From proto-neutron star dynamo to low-field magnetars, <https://arxiv.org/abs/2501.04768>
- Isayev, A. A. 2014, *Int. J. Mod. Phys. A*, 29, 1450173, doi: [10.1142/S0217751X14501735](https://doi.org/10.1142/S0217751X14501735)
- Jiang, J.-L., Ng, H. H.-Y., Chabanov, M., & Rezzolla, L. 2025, <https://arxiv.org/abs/2502.14962>
- Kaspi, V. M., & Beloborodov, A. 2017, *Ann. Rev. Astron. Astrophys.*, 55, 261, doi: [10.1146/annurev-astro-081915-023329](https://doi.org/10.1146/annurev-astro-081915-023329)
- Kastaun, W., Kalinani, J. V., & Cioffi, R. 2021, *Phys. Rev. D*, 103, 023018, doi: [10.1103/PhysRevD.103.023018](https://doi.org/10.1103/PhysRevD.103.023018)
- Kawaguchi, M., Siddique, I., & Huang, M. 2025, *Eur. Phys. J. C*, 85, 246, doi: [10.1140/epjc/s10052-025-13952-1](https://doi.org/10.1140/epjc/s10052-025-13952-1)
- Kawamura, T., Giacomazzo, B., Kastaun, W., et al. 2016, *Phys. Rev. D*, 94, 064012, doi: [10.1103/PhysRevD.94.064012](https://doi.org/10.1103/PhysRevD.94.064012)
- Kiuchi, K. 2025, General Relativistic Magnetohydrodynamics Simulations for Binary Neutron Star Mergers, ed. C. Bambi, Y. Mizuno, S. Shashank, & F. Yuan (Singapore: Springer Nature Singapore), 529–572, doi: [10.1007/978-981-97-8522-3_16](https://doi.org/10.1007/978-981-97-8522-3_16)
- Kiuchi, K., Cerdá-Durán, P., Kyutoku, K., Sekiguchi, Y., & Shibata, M. 2015, *Phys. Rev. D*, 92, 124034, doi: [10.1103/PhysRevD.92.124034](https://doi.org/10.1103/PhysRevD.92.124034)
- Kiuchi, K., Kyutoku, K., Sekiguchi, Y., & Shibata, M. 2018, *Phys. Rev. D*, 97, 124039, doi: [10.1103/PhysRevD.97.124039](https://doi.org/10.1103/PhysRevD.97.124039)
- Kiuchi, K., Kyutoku, K., Sekiguchi, Y., Shibata, M., & Wada, T. 2014, *Phys. Rev. D*, 90, 041502, doi: [10.1103/PhysRevD.90.041502](https://doi.org/10.1103/PhysRevD.90.041502)
- Kiuchi, K., Reboul-Salze, A., Shibata, M., & Sekiguchi, Y. 2024, *Nature Astron.*, 8, 298, doi: [10.1038/s41550-024-02194-y](https://doi.org/10.1038/s41550-024-02194-y)

- Lalazissis, G. A., Konig, J., & Ring, P. 1997, *Phys. Rev. C*, 55, 540, doi: [10.1103/PhysRevC.55.540](https://doi.org/10.1103/PhysRevC.55.540)
- Lander, S. K., Haensel, P., Haskell, B., Zdunik, J. L., & Fortin, M. 2021, *Mon. Not. Roy. Astron. Soc.*, 503, 875, doi: [10.1093/mnras/stab460](https://doi.org/10.1093/mnras/stab460)
- Lattimer, J. M., Pethick, C. J., Ravenhall, D. G., & Lamb, D. Q. 1985, *Nucl. Phys. A*, 432, 646, doi: [10.1016/0375-9474\(85\)90006-5](https://doi.org/10.1016/0375-9474(85)90006-5)
- Lattimer, J. M., & Swesty, F. D. 1991, *Nucl. Phys. A*, 535, 331, doi: [10.1016/0375-9474\(91\)90452-C](https://doi.org/10.1016/0375-9474(91)90452-C)
- Lo, P. M., Szymański, M., Sasaki, C., & Redlich, K. 2020, *Phys. Rev. D*, 102, 034024, doi: [10.1103/PhysRevD.102.034024](https://doi.org/10.1103/PhysRevD.102.034024)
- Loffler, F., et al. 2012, *Class. Quant. Grav.*, 29, 115001, doi: [10.1088/0264-9381/29/11/115001](https://doi.org/10.1088/0264-9381/29/11/115001)
- Lu, Z.-Y., Xu, J.-F., Wen, X.-J., Peng, G.-X., & Ruggieri, M. 2022, *Chin. Phys. C*, 46, 064104, doi: [10.1088/1674-1137/ac5513](https://doi.org/10.1088/1674-1137/ac5513)
- Lugones, G., & Grunfeld, A. G. 2019, *Phys. Rev. C*, 99, 035804, doi: [10.1103/PhysRevC.99.035804](https://doi.org/10.1103/PhysRevC.99.035804)
- Maeder, A., & Meynet, G. 2003, *Astron. Astrophys.*, 411, 543, doi: [10.1051/0004-6361:20031491](https://doi.org/10.1051/0004-6361:20031491)
- Makishima, K., Enoto, T., Hiraga, J. S., et al. 2014, *Phys. Rev. Lett.*, 112, 171102, doi: [10.1103/PhysRevLett.112.171102](https://doi.org/10.1103/PhysRevLett.112.171102)
- Makishima, K., Enoto, T., Yoneda, H., & Odaka, H. 2021, *Mon. Not. Roy. Astron. Soc.*, 502, 2266, doi: [10.1093/mnras/stab149](https://doi.org/10.1093/mnras/stab149)
- Makishima, K., Murakami, H., Enoto, T., & Nakazawa, K. 2019, *Publ. Astron. Soc. Jap.*, 71, Publications of the Astronomical Society of Japan, Volume 71, Issue 1, 1 January 2019, 15, <https://doi.org/10.1093/pasj/psy129>, doi: [10.1093/pasj/psy129](https://doi.org/10.1093/pasj/psy129)
- Makishima, K., Uchida, N., & Enoto, T. 2024, *Observational Clues to the Magnetic Evolution of Magnetars*, <https://arxiv.org/abs/2407.15409>
- Margalit, B., Jermyn, A. S., Metzger, B. D., Roberts, L. F., & Quataert, E. 2022, *Astrophys. J.*, 939, 51, doi: [10.3847/1538-4357/ac8b01](https://doi.org/10.3847/1538-4357/ac8b01)
- Margalit, B., & Metzger, B. D. 2017, *Astrophys. J. Lett.*, 850, L19, doi: [10.3847/2041-8213/aa991c](https://doi.org/10.3847/2041-8213/aa991c)
- Metzger, B. D., Thompson, T. A., & Quataert, E. 2018, *Astrophys. J.*, 856, 101, doi: [10.3847/1538-4357/aab095](https://doi.org/10.3847/1538-4357/aab095)
- Miravet-Tenés, M., Guerra, D., Ruiz, M., Cerdá-Durán, P., & Font, J. A. 2024, *Identifying thermal effects in neutron star merger remnants with model-agnostic waveform reconstructions and third-generation detectors*, <https://arxiv.org/abs/2401.02493>
- Mishra, A., Singh, A. K., Rawat, N. S., & Aman, P. 2019, *Eur. Phys. J. A*, 55, 107, doi: [10.1140/epja/i2019-12783-5](https://doi.org/10.1140/epja/i2019-12783-5)
- Mondal, R., Chaudhuri, N., Roy, P., & Sarkar, S. 2024a, *Phys. Rev. C*, 109, 054911, doi: [10.1103/PhysRevC.109.054911](https://doi.org/10.1103/PhysRevC.109.054911)
- Mondal, R., Duari, S., Chaudhuri, N., Sarkar, S., & Roy, P. 2024b, *Phys. Rev. D*, 110, 054010, doi: [10.1103/PhysRevD.110.054010](https://doi.org/10.1103/PhysRevD.110.054010)
- Most, E. R. 2023, *Impact of a mean field dynamo on neutron star mergers leading to magnetar remnants*, doi: [10.1103/PhysRevD.108.123012](https://doi.org/10.1103/PhysRevD.108.123012)
- Most, E. R., Haber, A., Harris, S. P., et al. 2024, *Astrophys. J. Lett.*, 967, L14, doi: [10.3847/2041-8213/ad454f](https://doi.org/10.3847/2041-8213/ad454f)
- Most, E. R., & Noronha, J. 2021, *Phys. Rev. D*, 104, 103028, doi: [10.1103/PhysRevD.104.103028](https://doi.org/10.1103/PhysRevD.104.103028)
- Most, E. R., Papenfort, L. J., & Rezzolla, L. 2019, *Mon. Not. Roy. Astron. Soc.*, 490, 3588, doi: [10.1093/mnras/stz2809](https://doi.org/10.1093/mnras/stz2809)
- Most, E. R., Papenfort, L. J., Weih, L. R., & Rezzolla, L. 2020, *Mon. Not. Roy. Astron. Soc.*, 499, L82, doi: [10.1093/mnras/slaa168](https://doi.org/10.1093/mnras/slaa168)
- Most, E. R., & Quataert, E. 2023, *Astrophys. J. Lett.*, 947, L15, doi: [10.3847/2041-8213/acca84](https://doi.org/10.3847/2041-8213/acca84)
- Most, E. R., & Raithel, C. A. 2021, *Phys. Rev. D*, 104, 124012, doi: [10.1103/PhysRevD.104.124012](https://doi.org/10.1103/PhysRevD.104.124012)
- Most, E. R., Weih, L. R., Rezzolla, L., & Schaffner-Bielich, J. 2018, *Phys. Rev. Lett.*, 120, 261103, doi: [10.1103/PhysRevLett.120.261103](https://doi.org/10.1103/PhysRevLett.120.261103)
- Most, E. R., Harris, S. P., Plumberg, C., et al. 2021, *Mon. Not. Roy. Astron. Soc.*, 509, 1096, doi: [10.1093/mnras/stab2793](https://doi.org/10.1093/mnras/stab2793)
- Mösta, P., Radice, D., Haas, R., Schnetter, E., & Bernuzzi, S. 2020, *Astrophys. J. Lett.*, 901, L37, doi: [10.3847/2041-8213/abb6ef](https://doi.org/10.3847/2041-8213/abb6ef)
- Mueller, H., & Serot, B. D. 1996, *Nucl. Phys. A*, 606, 508, doi: [10.1016/0375-9474\(96\)00187-X](https://doi.org/10.1016/0375-9474(96)00187-X)
- Musolino, C., Rezzolla, L., & Most, E. R. 2024, <https://arxiv.org/abs/2410.06253>
- Nathanail, A., Most, E. R., & Rezzolla, L. 2021, *Astrophys. J. Lett.*, 908, L28, doi: [10.3847/2041-8213/abdfc6](https://doi.org/10.3847/2041-8213/abdfc6)
- Nedora, V., Radice, D., Bernuzzi, S., et al. 2021, *Mon. Not. Roy. Astron. Soc.*, 506, 5908, doi: [10.1093/mnras/stab2004](https://doi.org/10.1093/mnras/stab2004)
- Noronha, J., Spaliński, M., & Speranza, E. 2022, *Phys. Rev. Lett.*, 128, 252302, doi: [10.1103/PhysRevLett.128.252302](https://doi.org/10.1103/PhysRevLett.128.252302)
- Orsaria, M., Ranea-Sandoval, I. F., & Vucetich, H. 2011, *Astrophys. J.*, 734, 41, doi: [10.1088/0004-637X/734/1/41](https://doi.org/10.1088/0004-637X/734/1/41)
- Pais, H., Bertolino, B., Fang, J., Wang, X., & Providência, C. 2021, *Eur. Phys. J. A*, 57, 193, doi: [10.1140/epja/s10050-021-00506-8](https://doi.org/10.1140/epja/s10050-021-00506-8)
- Pais, H., Chiacchiera, S., & Providência, C. 2015, *Phys. Rev. C*, 91, 055801, doi: [10.1103/PhysRevC.91.055801](https://doi.org/10.1103/PhysRevC.91.055801)

- Pais, H., & Providência, C. 2016, *Phys. Rev. C*, 94, 015808, doi: [10.1103/PhysRevC.94.015808](https://doi.org/10.1103/PhysRevC.94.015808)
- Palenzuela, C., Liebling, S., & Miñano, B. 2022, *Phys. Rev. D*, 105, 103020, doi: [10.1103/PhysRevD.105.103020](https://doi.org/10.1103/PhysRevD.105.103020)
- Palenzuela, C., Liebling, S. L., Neilsen, D., et al. 2015, *Phys. Rev. D*, 92, 044045, doi: [10.1103/PhysRevD.92.044045](https://doi.org/10.1103/PhysRevD.92.044045)
- Papazoglou, P., Schramm, S., Schaffner-Bielich, J., Stoecker, H., & Greiner, W. 1998, *Phys. Rev. C*, 57, 2576, doi: [10.1103/PhysRevC.57.2576](https://doi.org/10.1103/PhysRevC.57.2576)
- Papenfort, L. J., Tootle, S. D., Grandclément, P., Most, E. R., & Rezzolla, L. 2021, *Phys. Rev. D*, 104, 024057, doi: [10.1103/PhysRevD.104.024057](https://doi.org/10.1103/PhysRevD.104.024057)
- Perego, A., Bernuzzi, S., & Radice, D. 2019, *Eur. Phys. J. A*, 55, 124, doi: [10.1140/epja/i2019-12810-7](https://doi.org/10.1140/epja/i2019-12810-7)
- Peterson, J., Costa, P., Kumar, R., et al. 2023, *Phys. Rev. D*, 108, 063011, doi: [10.1103/PhysRevD.108.063011](https://doi.org/10.1103/PhysRevD.108.063011)
- Pimentel, O. M., Lora-Clavijo, F. D., & González, G. A. 2018, *Astrophys. J.*, 861, 115, doi: [10.3847/1538-4357/aac6d0](https://doi.org/10.3847/1538-4357/aac6d0)
- Pons, J. A., & Viganò, D. 2019, *Living Reviews in Computational Astrophysics*, 5, 1
- Potekhin, A. Y., & Chabrier, G. 2018, *Astron. Astrophys.*, 609, A74, doi: [10.1051/0004-6361/201731866](https://doi.org/10.1051/0004-6361/201731866)
- Prasad, R., & Mallick, R. 2022, *Mon. Not. Roy. Astron. Soc.*, 516, 1127, doi: [10.1093/mnras/stac2324](https://doi.org/10.1093/mnras/stac2324)
- Price, D., & Rosswog, S. 2006, Producing ultra-strong magnetic fields in neutron star mergers, doi: [10.1126/science.1125201](https://doi.org/10.1126/science.1125201)
- Raithel, C., Özel, F., & Psaltis, D. 2018, *Astrophys. J. Lett.*, 857, L23, doi: [10.3847/2041-8213/aabcbf](https://doi.org/10.3847/2041-8213/aabcbf)
- Raithel, C., Paschalidis, V., & Özel, F. 2021, *Phys. Rev. D*, 104, 063016, doi: [10.1103/PhysRevD.104.063016](https://doi.org/10.1103/PhysRevD.104.063016)
- Raithel, C. A., & Most, E. R. 2022, *Astrophys. J. Lett.*, 933, L39, doi: [10.3847/2041-8213/ac7c75](https://doi.org/10.3847/2041-8213/ac7c75)
- Raithel, C. A., & Paschalidis, V. 2023, *Phys. Rev. D*, 108, 083029, doi: [10.1103/PhysRevD.108.083029](https://doi.org/10.1103/PhysRevD.108.083029)
- Raithel, C. A., & Paschalidis, V. 2024, *Phys. Rev. D*, 110, 043002, doi: [10.1103/PhysRevD.110.043002](https://doi.org/10.1103/PhysRevD.110.043002)
- Raynaud, R., Guilet, J., Janka, H.-T., & Gastine, T. 2020, *Sci. Adv.*, 6, eaay2732, doi: [10.1126/sciadv.aay2732](https://doi.org/10.1126/sciadv.aay2732)
- Reboul-Salze, A., Barrère, P., Kiuchi, K., et al. 2024, <https://arxiv.org/abs/2411.19328>
- Rezzolla, L., Most, E. R., & Weih, L. R. 2018, *Astrophys. J. Lett.*, 852, L25, doi: [10.3847/2041-8213/aaa401](https://doi.org/10.3847/2041-8213/aaa401)
- Rocha, G. S., & Denicol, G. S. 2021, *Phys. Rev. D*, 104, 096016, doi: [10.1103/PhysRevD.104.096016](https://doi.org/10.1103/PhysRevD.104.096016)
- Romatschke, P. 2010, *Int. J. Mod. Phys. E*, 19, 1, doi: [10.1142/S0218301310014613](https://doi.org/10.1142/S0218301310014613)
- Ruiz, M., Shapiro, S. L., & Tsokaros, A. 2018, *Phys. Rev. D*, 97, 021501, doi: [10.1103/PhysRevD.97.021501](https://doi.org/10.1103/PhysRevD.97.021501)
- Scurto, L., Carvalho, V., Pais, H., & Providência, C. 2024, *Phys. Rev. C*, 110, 045805, doi: [10.1103/PhysRevC.110.045805](https://doi.org/10.1103/PhysRevC.110.045805)
- Scurto, L., Pais, H., & Gulminelli, F. 2023, *Phys. Rev. C*, 107, 045806, doi: [10.1103/PhysRevC.107.045806](https://doi.org/10.1103/PhysRevC.107.045806)
- Serot, B. D., & Walecka, J. D. 1986, *Adv. Nucl. Phys.*, 16, 1
- Shapiro, S. L. 2000, *Astrophys. J.*, 544, 397, doi: [10.1086/317209](https://doi.org/10.1086/317209)
- Shibata, M., Zhou, E., Kiuchi, K., & Fujibayashi, S. 2019, *Phys. Rev. D*, 100, 023015, doi: [10.1103/PhysRevD.100.023015](https://doi.org/10.1103/PhysRevD.100.023015)
- Sinha, M., Huang, X.-G., & Sedrakian, A. 2013, *Phys. Rev. D*, 88, 025008, doi: [10.1103/PhysRevD.88.025008](https://doi.org/10.1103/PhysRevD.88.025008)
- Strickland, M., Dexheimer, V., & Menezes, D. P. 2012, *Phys. Rev. D*, 86, 125032, doi: [10.1103/PhysRevD.86.125032](https://doi.org/10.1103/PhysRevD.86.125032)
- Suvorov, A. G., & Pons, J. A. 2025, <https://arxiv.org/abs/2503.01409>
- Tan, H., Noronha-Hostler, J., & Yunes, N. 2020, *Phys. Rev. Lett.*, 125, 261104, doi: [10.1103/PhysRevLett.125.261104](https://doi.org/10.1103/PhysRevLett.125.261104)
- Tolos, L., Centelles, M., & Ramos, A. 2017, *Astrophys. J.*, 834, 3, doi: [10.3847/1538-4357/834/1/3](https://doi.org/10.3847/1538-4357/834/1/3)
- Tsokaros, A., Bamber, J., Ruiz, M., & Shapiro, S. L. 2025, *Phys. Rev. Lett.*, 134, 121401, doi: [10.1103/PhysRevLett.134.121401](https://doi.org/10.1103/PhysRevLett.134.121401)
- Villa-Ortega, V., Lorenzo-Medina, A., Calderón Bustillo, J., et al. 2023, Self-consistent treatment of thermal effects in neutron-star post-mergers: observational implications for third-generation gravitational-wave detectors, <https://arxiv.org/abs/2310.20378>
- Virtanen, P., Gommers, R., Oliphant, T. E., et al. 2020, *Nature Methods*, 17, 261, doi: [10.1038/s41592-019-0686-2](https://doi.org/10.1038/s41592-019-0686-2)
- Wang, X., Li, J., Fang, J., Pais, H., & Providência, C. 2022, *Phys. Rev. D*, 105, 063004, doi: [10.1103/PhysRevD.105.063004](https://doi.org/10.1103/PhysRevD.105.063004)
- Wang, Y., & Wen, X.-J. 2024, *Phys. Rev. C*, 109, 015201, doi: [10.1103/PhysRevC.109.015201](https://doi.org/10.1103/PhysRevC.109.015201)
- Wheeler, J. C., Meier, D. L., & Wilson, J. R. 2002, *Astrophys. J.*, 568, 807, doi: [10.1086/338953](https://doi.org/10.1086/338953)
- Zappa, F., Bernuzzi, S., Radice, D., & Perego, A. 2022, Binary neutron star merger simulations with neutrino transport and turbulent viscosity: impact of different schemes and grid resolution, doi: [10.1093/mnras/stad107](https://doi.org/10.1093/mnras/stad107)
- Zlochower, Y., Baker, J. G., Campanelli, M., & Lousto, C. O. 2005, *Phys. Rev. D*, 72, 024021, doi: [10.1103/PhysRevD.72.024021](https://doi.org/10.1103/PhysRevD.72.024021)
- Zyla, P. A., et al. 2020, *PTEP*, 2020, 083C01, doi: [10.1093/ptep/ptaa104](https://doi.org/10.1093/ptep/ptaa104)